Response to reviewers comments for the paper “**Downwind evolution of the volatility and mixing state of near-road aerosols near a US interstate highway**” by Provat K. Saha et al.

To Whom It May Concern:

We would like to thank the two reviewers for their thoughtful and helpful comments. In addressing these comments, we feel we have substantially improved the manuscript.

Please find below detailed responses shown in **blue text (**with direct quotes from the revised manuscript shown in *italics*) to the comments and suggestions offered by the two reviewers. The changes made in the revised manuscript and SI are marked-up with blue text as well.

Best regards,

The Authors

Anonymous Referee #1

In this study, the authors report composition, volatility and mixing state of traffic-related aerosols measured near a highway, 10 m to 220 m from the road edge. Measurements were conducted under varied environmental conditions including winter and summer campaigns. The investigation is important because vehicle emissions undergo a rapid transformation in ambient air which influences the key properties of combustion emissions with respect to their health and environmental effects. The data provided by this work is valuable and data-analysis is ambitious. Especially, this manuscript offers a high-quality data about the volatility distribution of traffic emissions. The topic is fitting well in the scope of ACP. Revised manuscript is suitable for publication in ACP after following comments are addressed:

We thank the reviewer for the encouraging comments.

The last paragraph of chapter 3.4 (tracer m/z based factor analysis) should be shortened. Perhaps, this paragraph could be moved to the supplement. Did you use estimation HOA = 13.4 × (C57 - 0.1 × C44) (Ng et al., 2011)? I would recommend using PMF (Ulbrich et al., 2009) instead of tracer-based factor analysis, if possible.

Following the reviewer’s suggestion, we revisited the last paragraph of section 3.4. The details on tracer m/z based analysis and the corresponding discussion are moved to the supplement (see Sec. S5: Tracer m/z based factor analysis of ACSM dataset) and this analysis is now only briefly mentioned in the main text. As the reviewer inferred, tracer m/z based OA components are estimated following Ng et al. (2011) as: hydrocarbon-like OA (HOA ~ $13.4 \times (C_{57} - 0.1 \times C_{44})$) and oxygenated OA (OOA ~ $6.6 \times C_{44}$), where C_{57} and C_{44} are the equivalent mass concentration of tracer ion m/z 57 and 44, respectively. Previous evaluation of this method has shown that it can reproduce the HOA and OOA concentrations to within ~30% of the results from detailed PMF analysis (Ng. et al. 2011). A detailed PMF analysis of this data set would require an extensive new analysis and thus we considering it beyond the scope of this manuscript. Further, since the estimated traffic-OA (HOA factor) contribution was found to be ~5-10x lower than that derived based on background-subtracted roadside concentrations measured by SMPS, we do not expect that a detailed PMF analysis will close this gap. We have discussed several factors that likely contribute to this discrepancy.

Revision: Please see revised SI, Sec. *S5: Tracer m/z based factor analysis of ACSM data set.*

Figure 8: Figure 8 is quite hard to read and should be improved e.g. by adding summer and winter volatility distributions (Table 1) to Fig. 8b for comparison and clarify figure caption. If bins 2-6 (Table 1) are not applied in this work, please, consider removing these bins from Table 1 (or add marking for these).

We thank the reviewer for paying special attention to Fig. 8, and we agree that some clarification is needed. One thing requiring clarification is that the purpose of the analysis in Fig. 8 is *not* to show the volatility distributions from summer and winter. We show simplified versions of the volatility distributions from summer and winter at different distances from the highway in Fig. 7 and the full distributions are listed in table 1. The purpose of the analysis resulting in Fig. 8 was to examine how well a laboratory-measured volatility distribution of traffic POA (May et al., 2013) can explain the observed partitioning of vehicle emissions in a complex near-road environment. In this analysis, we hypothesized that the volatility distribution of road-side OA results from a superposition/weighted average of the volatility distributions of traffic-contributed OA and background OA. We compare our measured road-side volatility distribution (at 10 m) with a reconstructed distribution using the volatility distribution from laboratory vehicle measurements described in May et al. (2013) and the 'background' distribution measured at our furthest-from-road location (220 m). In the revised manuscript, we tried to clarify the discussion of Fig. 8 by changing the figure caption and legend, adding markers to the figure, improving the text description and adding a new supporting section in SI (sec. S4) that describes the analysis approach step-by step.

Revision: Please see (i) revised Fig. 8, (ii) revised text in Sec. 3.4 and (iii) new addition of Sec. S4 in SI

Fig S3: Size distributions of nucleation mode particles look odd. Please, check SMPS data carefully, especially particles smaller than 10 nm

We thank the reviewer for taking a close look at this Figure and pointing out this issue. Fig.S3 showed example data from a typical transect measurement to demonstrate the relative change in particle number distributions at different distances from the highway. Data were collected using an SMPS system with a TSI 3010 CPC, which has a detection limit (lower size cut) of 10 nm. Therefore, counting for particles smaller than 10 nm was distorted and should have been excluded from the original figure. In revision, we show a similar example data set from another transect run with data below 10 nm excluded. We mainly made this change to include an example that more clearly demonstrates, in a relative sense, the strong spatial gradient of PN size distribution above 10 nm.

Revision: Please see revised Figure S3

- Fig S7: AN and AS mass concentrations (calculation) based on a statement that aerosols are neutral. Please, add acidity plot (NH4 measured vs. NH4 calculated) to prove that assumption (Supplement) or use model such as Aerosol Inorganic Model II (AIM-II) (Clegg et al., 1998) for acidity calculation. An effective density calculation (Kuwata et al., 2012) of OA is limited to particle components having negligible quantities of additional elements. How traffic emissions components such as black carbon and NO3 effect on density calculations?

An acidity plot (of measured vs. predicted NH_4) has been added as Fig. S7, panel (b). The NH4 predicted is estimated as: NH4 predicted = 2*(18/98)*SO4 + (18/63)*NO3 + (18/35)*Cl, where the fractional amounts correspond to the molecular weights of the relevant species. An ammonium balance can provide insights into the validity of assumption of neutral aerosol. Since the acidity plot (of measured vs. predicted NH4) has an average slope closer to ~1 (1.1±0.03), indicating an ammonium balance. Therefore, assumption of neutral aerosols at the measurement location was reasonable.

We agree that it is important to note the limitations associated with the application of the Kuwata et al. (2012) parameterization for OA density, which was developed based on laboratory data with negligible BC or nitrogen content. However, we are unable to comment on the extent to which this deviation will affect the density calculated in this way. We do note that Kuwata et al. applied their parameterization to data from the AMAZE campaign, which had an average OA fraction of 0.8 (versus 0.74 for our data), and found that the results agreed well with their measured density. Therefore, and given that we found the overall OA mass at this site to be dominated by relatively oxidized (OOA-like) spectra, we suspect that this parameterization does a reasonably good job describing our OA density. Therefore, we do not expect that the use of the Kuwata et al. (2012) parameterization, which assumes particle components having negligible quantities of additional elements, would introduce any dramatic bias. As noted elsewhere, we calculated the overall effective density of PM by weighting fractional contribution of major PM species (OA, BC, AN, and AS) with their respective densities; effective density of submicron PM = dens of OA $\times f_{OA}$ + dens of BC $\times f_{BC}$ + dens of AN $\times f_{AN}$ + dens of AS $\times f_{AS}$. The campaign average fractional contributions are OA ~74%, AS ~13%, AN ~7%, and BC ~6%. The density of OA is calculated using the Kuwata et al. (2012) parameterization, which depends on the molecular composition of OA (O:C, H:C). OA was the dominant component of measured PM (~ 75%) and overall contribution of traffic emitted inorganic components (~ BC) was relatively small (BC~ 6%). Finally, since our mass comparison based on application of this density to SMPS-measured volume and ACSM+BC mass showed good agreement (Fig. S7a), this indicates our overall estimated effective density, on which OA density has the largest influence, is well constrained.

Revision: Please see revised Figure S7 and text in caption.

Anonymous Referee #2

The authors present a dataset of aerosol evaporation in thermodenuders and ACSM and black carbon measurements measured at several distances from a major highway. The dataset and the associated analysis of the volatility and the mixing state of the aerosol at different distances downwind of the road is very valuable to atmospheric aerosol and traffic emission researchers. The measurements are to my knowledge the first time the volatility and mixing state have been measured at several points along the roadside, and as such the dataset is novel and interesting, and the subject area is clearly in line with ACP. The manuscript is well written and the data analysis is comprehensive; there are some issues that I suggest are addressed in a revision, after which I recommend publication.

We thank the reviewer for their encouraging comments

1. As the traffic-originated aerosol is transported away from the source, it dilutes with background aerosol with a rate that depends on the wind velocity and the atmospheric stability. Therefore, the same measurement point (measured by distance) can see aerosol with different age since emission, and different dilution factors. This can be overcome by measurements of some relatively inert gas at the roadside and downwind, or more crudely just estimating the aerosol ’age’ from the wind velocity, distance (and direction). Neither of these have been performed in the manuscript, and therefore the measurement at each distance may include differently aged particles, with a varying fraction of background aerosol mixed in the traffic-originated aerosol. This impacts the generalization of the results (which may easily happen, given the scarcity of this type of data in the literature), and I think that this should be made clear to readers. This could be done e.g. by providing estimates, and ranges of variation, of the age of particles as an additional variable. Also, this would give more confidence in whether the observed seasonal differences are due to actual differences in volatility or maybe just different mixing situations.

It is true that meteorological conditions (e.g., temperature, dilution) affect the transport and transformation of traffic plume in a near-road environment, thus can affect the volatility of transported particles. These effects were visible in our volatility measurements and extracted volatility distributions from two seasons, as discussed in Sec. 3.1 (page 8, L 5-15) and Sec. 3.3 (Page 12, L17-25). In a companion paper (Saha et al., 2017), we discussed the climatological aspects and transport of traffic plumes in detail. We observed a substantial seasonal difference in downwind decay profile of NO_x and BC (traffic tracer), and so we are able to comment on the relative difference in dilution and ‘age’ of sampled particles. In this paper we use BC as a ‘tracer’ in this way in several places (e.g. Fig. 2 and related discussion). A modified version of a figure from Saha et al. (2017) with a number of ‘tracers’ measured near the road (NOx, and BC) is shown below for reference. *Within* a given season, we did not observe a substantial day-to-day variability in pollutant profile, possibly because we conducted our transect measurements on a few days selected based on favorable weather conditions (with the wind coming off of the roadway). Since we discussed the different climatological aspects of our site and data in our companion paper (which will hopefully be published soon), we did not include it here. However here, and in the manuscript, we provide a basic description.

Winter measurements typically showed less rapid dilution (more stable conditions, lower wind speeds) and lower temperatures than the summer. Therefore, decay and mixing of the traffic plume was substantially slower in winter than in summer, as demonstrated by less steep downwind decay profiles of NOx and BC (traffic tracer) in winter than summer (see Fig. below). We observed the effects of these differences (temperature, dilution) in volatility distributions derived from the two seasons' data, as discussed in Sec. 3.3.

For example, we mention in Sec. 3.3 (page 12, L23-25). “*Atmospheric dilution was substantially lower in winter at our site (and generally) due to more stable atmospheric conditions under the colder weather (Saha et al., 2017a). Therefore, when comparing particle volatility at the same temperature, lower dilution during winter likely explains the observed higher SVOCs fraction*.”

In reality, the combined effects of temperature, dilution, and changes in tailpipe emission properties likely dictate the observed inter-seasonal differences in particle volatility. Although a complete decoupling each of these effects is challenging, our analysis indicates that the temperature effect is more important than others on the volatility distribution (e.g. Figs. 7, S11). The impact of dilution is less dramatic than temperature (Fig. 7 vs. Fig. S11) and a seasonal difference in tailpipe emission properties is likely also less important than the influence of ambient temperature on emission partitioning.

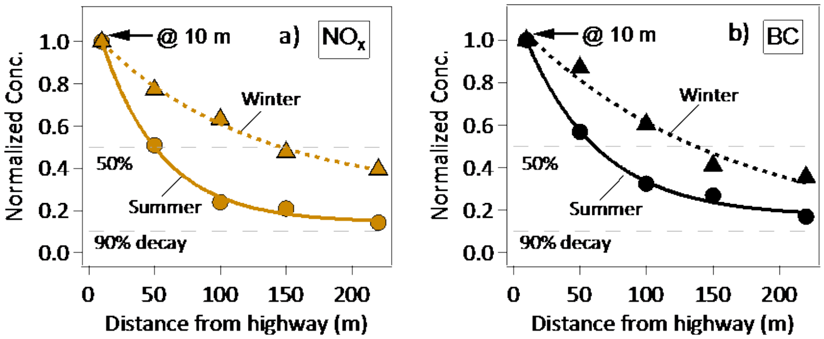

Figure showing **c**ampaign-average normalized downwind decay profile for a) NO_x, b) BC during summer and winter.

2. Comparing the distributions in Fig S3, it seems that an important factor in the change of volatility is the disappearance of a large fraction of particles smaller than ca 40-50 nm between the measurement points at 10 m and 150 m, and this seems to contribute to the large change in volatility of <100 nm particles (the change seems much less for the 100-400 nm particles). From this one could assume that these small particles are mostly consisting of SV particles. On the other hand, these smallest particles are most affected by e.g. coagulation, and their mass could thus be transferred to the larger size range during transport. I think that the large change with transport in the <50 nm particle size range should be investigated, and maybe some overview of the literature on whether this is a typical occurrence could be added to the paper.

We agree with the reviewer that other processes, including coagulation, should be considered as possibly important influences on near-road aerosol size distribution. Zhang et al. (2004) reported that after the initial stage of dilution (tailpipe to on-road), the second phase (road-to-ambient) aerosol size distribution evolution is dominated by condensation and dilution, while coagulation and deposition play minor roles. Choi and Paulson (2016) reported that only 5-10% of particle number concentration loss could be attributed to coagulation within 200 m from the roadway. Therefore, based on the evidence from existing literature, we do not expect that coagulation is a primary process in altering the physio-chemical properties of transported traffic particles within the near-road domain (10-200 m from the highway edge) where we conducted our measurements.

Revision: We included the following discussion (Page 7 L30 -Page 8 L3):

"It can be noted here that other processes, including coagulation, can possibly have important influences on the evolution of near-road aerosol size distribution. However, Zhang et al. (2004) reported that after the initial stage of dilution (tailpipe to on-road), the second phase (road-to-ambient) aerosol size distribution evolution is dominated by condensation and dilution, while coagulation and deposition play minor roles. Therefore, we do not expect that coagulation is a dominant process in altering the physio-chemical properties of transported traffic particles within the near-road domain (10-200 m from the highway edge) where we conducted our measurements."

As we discuss in Sec. 3.3 and Fig. 6, our results show that a single volatility distribution can explain the observed evaporation of different size particles at a given location for the size range we investigated (25-100 nm). Therefore, our analysis suggests that particles within this size range (25-100 nm) have a consistent volatility distribution or chemical signature, although they showed a different degree of evaporation in TD. This will also be true of evaporation due to atmospheric dilution. Typically, it is expected that very small particles will evaporate more quickly due to the Kelvin effect and increased surface/volume ratio, even if they have similar volatility distribution.

page 8, line 15: ’Other effects (if any)...’ This sentence is mostly confusing; either the other effects are clearly mentioned here, or this sentence could be removed.

Here, by ‘other effects (if any)’ we mean if there is any inter-seasonal differences in volatility. Revision: we revised this sentence as: “*Therefore, inter-seasonal differences in volatility of emissions (if any) should be reflected in the resulting fitted volatility distributions; these modeling results are discussed in Sec. 3.3.*” (Page 8, L18-19)

page 9, line 1: I’m not following what is meant by ’downwind trend is dictated by BC’. What is the BC-related process that determines the VFR? Also, it is not clear what the quantity VFR-OA is representing here. How is this related to the difference in BC and denuded SMPS volume in Fig. 2d? Also, is fig 2d an example or representative of a longer period? Please clarify.

We have made some minor edits to text in an effort to clarify this point. We’ll elaborate here, but hope the modified text conveys the point more clearly. We meant here that downwind evolution of VFR at 180 C follows the similar trend as BC. One approximation we can make that VFR at 180 C ~ ELVOC (extremely low-volatility organics) + BC. Since ELVOCs (~ OA MFR at very high temperature) are likely dominated by regional background aerosol, a gradient in the contribution from these species downwind of the roadway is not expected. Therefore, we would expect that near-road spatial gradient of PM VFR at a very high temperature will be dictated by the BC component. Our analysis in Fig. 2c supports this assumption: the scatter plot of [VFR at 180 C – ELVOC] vs. BC fraction has an average slope of 1.29±0.19. An alternative way of saying this is that the difference between high-temperature-TD-processed SMPS volume and BC should give us an estimate of ELVOCs. Fig. 2d indicates that this difference is ~ 65% of denuded SMPS volume at 180 C, and thus this fraction of PM volume may be considered as ELVOCs. This is consistent with our other measurement approach shown in Fig, 2b, showing that the OA MFR at 180 C measured via the ACSM at the roadside trailer is ~ 50% of PM VFR at 180 C. Therefore, by combining measurements from different instruments and approaches, the analysis in Fig. 2 indicates that in a near-road environment, denuded particle volume at very high temperature (180 C) can be approximated as~ ELVOCs + BC, and its spatial trend is dictated by BC component (traffic tracer), not changes in ELVOC content away from the roadway. All plots in Fig.2 show campaign-average observations (as mentioned in the caption), so these trends should be fairly representative.

Revision: To summarize and clarify the analyses is Fig 2, we added the following sentences (Page 9, L16-19): “*Therefore, by combining measurements from different instruments and approaches, the analysis summarized in Fig.2 indicates that in a near-road environment, denuded particle volume at very high temperature (at 180 C) can be approximated as~ ELVOCs + BC, with a spatial trend that is dictated by BC (as a traffic tracer).*”

Page 9, line 15, and Fig 3 and 5. The sentence ’The evolution of the size distribution of a monodisperse particle upon heating’ is confusing.

Revision: We revised this as: “*The heated size distributions of a size-selected monodisperse (at ambient temperature) aerosol at different TD temperature is referred to as a volatility spectra.*” (Page9, L21-22)

Also, how is the color scale chosen in Figs. 3 and 5? As the main information of the figure is the relative contributions of the different modes, could it not be useful to normalize the volatility spectra? Now the 25 nm spectra are very vaguely readable

The reviewer correctly points out that the primary information of the figure is the relative contributions of the different modes, and these data could be presented in a normalized form. However, we aimed to show the relative abundance of different size particles at a particular location, as well as how this changes with distance (especially for Fig. 5), and so choose to show absolute concentrations with the same color scale for all panels in Fig. 3 and 5. For example, the color scale in Fig. 5 allows us to show that concentrations of 100 nm particles reduced with distance, but their mixing state remained almost unchanged. We feel this is the best overall approach for displaying these data.

page 11, line 6: '...the mixing state of traffic-emitted particles is not substantially altered within a few hundred meters'. This is basically correct in the context that particles that are externally mixed at the start stay so; however, in a hypothetical case that internally mixed particles dominate the emission at the start, the mixing with background air would soon cause an external mixture. The sentence should be made less general, e.g. '...in this case, the mixing state...'

We thank the reviewer for the suggestion. One thing to make clear here is that we state that the mixing-state of traffic particles at near-road (10 m) and far-road (200 m) remained almost same, but we didn't indicate their degree of mixing. For example, if some percentage of BC particles from traffic emissions is externally mixed at the near-road location (10 m), their mixing state did not substantially alter within a few hundred meters. If traffic particles are internally mixed at the start (e.g., BC mixed with HOA), it will remain so during mixing with background air (since that already has some mixing/coating of OA). Essentially, the fraction of internally and externally mixed particles doesn't appear to change, nor is there evidence of substantial coating on externally mixed 'non-volatile' particles.

Revision: To make this sentence more specific, we revised it as: "*This result indicates that there is minimal change in the mixing state in traffic-emitted particles between the near-road (~10 m) and far-road (~220 m) locations. Specifically, the proportion of internally versus externally mixed particles doesn't appear to change, nor is there evidence of substantial coating on externally mixed 'non-volatile' particles.*" (Page 11, L12-15)

page 13, line 26, and Fig. 8. I have some difficulties understanding how Fig. 8b was arrived at, and what should be compared in the figure. Which bars at at 10m and which ones at 220? The statement 'we assume that the volatility distribution (...) at 220 is a representative (...) for background particles' seems contradicting to fig 8a, where ca 33% of the total aerosol seems to still be traffic-originated. I think that it would be helpful to understanding if a more detailed (step-by-step) explanation for how each of the three mass concentrations were obtained could be given, maybe even in equation form in the supplementary. For example:
M(near-road)i = (SMPS total mass - BC - ACSM(inorganics)) x (May et al)i
M(background)i = (bg OA mass) x (TD vol. distribution at 220m)i

M(traffic)i = (NR - BG oa mass) x (TD vol. distribution at 10 m)i

We thank the reviewer for these helpful suggestions. In response to this and the other reviewer's comment, we have made multiple efforts to improve the clarity of the analysis and discussion around Fig. 8. For example, by changing the figure caption and legend, adding tags to specific bars, making changes in the text and adding a new supporting section in SI. The main point of this analysis is a comparison of our measured road-side volatility distribution (at 10 m) with a reconstructed distribution using traffic and background. We added multiple arrows in the revised figure that should clarify what should be compared in this figure (i.e., measured vs. reconstructed distribution). Following the reviewer's suggestion, we added a new section in the SI (sec. S4) that provides a detailed (step-by-step) explanation on how each of the three distributions were estimated.

The reviewer correctly pointed out that at our far-road location a non-negligible fraction (~20-30%) of total aerosol is likely from traffic emissions in this particular case. However, since we do not have measurements of particle volatility at our upwind background site, the use of the measured distribution from the far-road location as 'background' was our best approximation. We have added text to make this caveat clear.

Since we did not measure particle volatility at our upwind background site, we assume that the volatility distribution measured at our far-from-road downwind location (220 m) is a representative distribution for background particles. This is a reasonable approximation as particle concentrations approach background levels within 200-300 m from the highway (Saha et al., 2017a). It should be noted that this 'background' OA contains a non-negligible (~25%) contribution from traffic emissions (Fig. 8a), and so likely has a slightly greater contribution from higher-volatility components than what would be measured in an actual 'background' location.

One should highlight here that volatility of traffic-particles at near-road and the far-road location are not expected to be the same. The distribution at far from the road (more diluted) is expected to be more 'background like.' Therefore, even though a small fraction of the aerosol in the far-road location can be from traffic origin, its overall effects on the background volatility distribution is not expected to be dramatic as substantial evolution has already occurred. We have added a caveat that more extensive modeling is needed to represent these processes.

While this simplified 'superposition' analysis suggests that our data are able to capture the influences of near-road evolution on emissions, further measurements and modelling work are needed to represent these dynamic processes.

Revision: For further details, please see (i) revised Fig. 8, (ii) revised text in MS Sec. 3.4 and (iii) new addition of Sec.S4 in SI

Several assumed densities could be found in the article for different data analysis approaches (at least 1.1, 1.5 and 1.8 g/cm3 are described). Could this be made more consistent, or are there specific reasons for using these values that could be stated?

We assume a density of 1.8 g/cm3 for BC particles for SP2 data analysis. We estimated an effective density of 1.5 g/cm3 for submicron PM (see Fig. S7 for details) for converting SMPS total volume to mass. A density of 1.1 g/cm3 (Table S1), was listed from May et al. (2013) along with different assumed TD kinetic model input parameters. However, since our TD kinetics modeling was based on tracking change in monodisperse particle size upon heating (V-TDMA approach), density does not play a role in the evolution of particle size. Therefore, we removed that entry from Table S1 to avoid confusion.

References

Choi, W. and Paulson, S. E.: Closing the ultrafine particle number concentration budget at road-to-ambient scale: Implications for particle dynamics, Aerosol Sci. Technol., 50(5), 448–461, doi:10.1080/02786826.2016.1155104, 2016.

Kuwata, M., Zorn, S. R. and Martin, S. T.: Using Elemental Ratios to Predict the Density of Organic Material Composed of Carbon, Hydrogen, and Oxygen, Environ. Sci. Technol., 46(2), 787–794, doi:10.1021/es202525q, 2012.

May, A. A., Presto, A. A., Hennigan, C. J., Nguyen, N. T., Gordon, T. D. and Robinson, A. L.: Gas-particle partitioning of primary organic aerosol emissions: (1) Gasoline vehicle exhaust, Atmos. Environ., 77, 128–139, doi:10.1016/j.atmosenv.2013.04.060, 2013.

Ng, N. L., Canagaratna, M. R., Jimenez, J. L., Zhang, Q., Ulbrich, I. M. and Worsnop, D. R.: Real-Time Methods for Estimating Organic Component Mass Concentrations from Aerosol Mass Spectrometer Data, Environ. Sci. Technol., 45(3), 910–916, doi:10.1021/es102951k, 2011.

Saha, P. K., Khlystov, A., Snyder, M. G. and Grieshop, A. P.: Characterization of air pollutant concentrations, fleet emission factors, and dispersion near a North Carolina interstate freeway across two seasons, Atmos. Environ., minor revisions, 2017.

Zhang, K. M., Wexler, A. S., Zhu, Y. F., Hinds, W. C. and Sioutas, C.: Evolution of particle number distribution near roadways. Part II: the “Road-to-Ambient” process, Atmos. Environ., 38(38), 6655–6665, doi:10.1016/j.atmosenv.2004.06.044, 2004.

Downwind evolution of the volatility and mixing state of near-road aerosols near a US interstate highway

Provat Kumar Saha[1], Andrey Khlystov[2], and Andrew Patrick Grieshop[1]

[1]Department of Civil, Construction and Environmental Engineering, North Carolina State University, Raleigh, North Carolina, USA
[2]Division of Atmospheric Sciences, Desert Research Institute, Reno, Nevada, USA

Correspondence to: A. P. Grieshop (apgriesh@ncsu.edu)

Abstract. We present spatial measurements of particle volatility and mixing state at a site near a North Carolina interstate highway (I-40) applying several heating (thermodenuder; TD) experimental approaches. Measurements were conducted in summer 2015 and winter 2016 in a roadside trailer (10 m from road edge) and during downwind transects at different distances from the highway under favorable wind conditions using a mobile platform. Results show that the relative abundance of semi-volatile species (SVOCs) in ultrafine particles decreases with downwind distance, consistent with the dilution and mixing of traffic-sourced particles with background air and evaporation of semi-volatile species during downwind transport. An evaporation kinetics model was used to derive particle volatility distributions by fitting TD data. While the TD-derived distribution apportions about 20-30% of particle mass as semi-volatile (SVOCs; effective saturation concentration, $C^* \geq 1\mu$ m-3) at 10 m from road edge, approximately 10% of particle mass is attributed to SVOCs at 220 m, showing that the particle-phase semi-volatile fraction decreases with downwind distance. The relative abundance of semi-volatile material in the particle-phase increased during winter. Downwind spatial gradients of the less-volatile particle fraction (that remaining after heating at 180°C) was strongly correlated with black carbon (BC). BC size distribution and mixing state measured using a Single Particle Soot Photometer (SP2) at the roadside trailer showed that a large fraction (70-80%) of BC particles were externally-mixed. Heating experiments with a volatility tandem differential mobility analyzer (V-TDMA) also showed that the non-volatile fraction in roadside aerosols are mostly externally mixed. V-TDMA measurements at different distances downwind from the highway indicate that mixing state of roadside aerosols does not change significantly (e.g., BC mostly remains externally mixed) within a few hundred meters from the highway. A preliminary analysis indicates that a super-position of volatility distributions measured in laboratory vehicle tests and of 'background' aerosol can be used to represent the observed partitioning of near-road particles. The results from this study highlight that exposures and impacts of BC and semi-volatile organics containing particles in a near-road microenvironment may differ across seasons and under changing ambient conditions.

1. Introduction

Motor vehicles are a large source of ambient fine particulate matter (PM) (Dallmann and Harley, 2010; Fraser et al., 1999; Kumar et al., 2011; Zhang et al., 2015). Particles emitted from vehicle exhaust are dominated by ultrafine particles (diameters < 100 nm) (Kleeman et al., 2000; Robert et al., 2007; Zhu et al., 2002), which are a concern due to their potential impacts on public health (Health Effects Institute, 2010; Hoek et al., 2009; Pope and Dockery, 2006). Vehicle-emitted PM largely consists of primary organic aerosol (POA) and black carbon (BC) (Dallmann et al., 2014; Maricq, 2007). Upon emission, vehicle exhaust undergoes rapid cooling and dilution with ambient air on the road. Emissions undergo further evolution from road to background-like conditions within a few hundred meters downwind from roadway (Robinson et al., 2010; Zhang et al., 2004), which involves complex physicochemical processes. Subsequently, size distribution and physio-chemical characteristics, and thus exposure characteristics and impacts, of aerosols evolve with downwind transport.

A large portion of POA emitted from motor vehicle is semivolatile material (Grieshop et al., 2009; May et al., 2013a; Presto et al., 2012) that can dynamically partition into the gas or particle phases with changing ambient conditions (e.g., temperature, concentrations) and atmospheric aging (Robinson et al., 2007, 2010). At equilibrium, the volatility of organic species (saturation vapor pressure, or equivalently, saturation concentration, C^*) dictates gas-particle partitioning (Donahue et al., 2006). Enthalpies of vaporization (ΔH_{vap}) also influences the change in partitioning with temperature (Epstein et al., 2010; Ranjan et al., 2012). Depending on the volatility of POA, and atmospheric perturbations (dilution, changing temperature), semi-volatile species in POA will dynamically partition into gas or particle phases as they move downwind. Therefore, gas-particle partitioning of POA likely plays an important role in determining human exposure to traffic emitted particles under varied ambient conditions.

Fresh BC particles emitted from vehicles are typically fractal in morphology (Bond et al., 2013; China et al., 2014) and may have varying size, shape and mixing state. BC may exist in the same particle as OA and others species (internally mixed) or in separate particles (externally mixed). The mixing state and morphology of BC particles can influence their radiative absorption properties (Cappa et al., 2012) and deposition in the human respiratory tract (Broday and Rosenzweig, 2011). The mixing state and physio-chemical characteristics of BC particles evolve as they undergo atmospheric processing and aging (Adachi and Buseck, 2013; Subramanian et al., 2010). For example, photochemical oxidation of volatile organic compounds (VOCs), intermediate-VOCs (IVOCs), and semi-volatile organic compounds (SVOCs) form condensable vapors. These condensable vapor can partition into the particle-phase either by absorbing into the organic condensed phase or adsorbing onto nonvolatile BC cores (Donahue et al., 2006; Pankow, 1994; Roth et al., 2005).

Spatial measurements of volatility and mixing state of near-road aerosols are critically important to better understand the evolution of vehicle-emitted POA and BC under diverse ambient conditions (e.g., seasons) as they are transported from roadways, to assess human exposure and health risks, and to improve their representation in air quality and exposure assessment models. Although a number of laboratory and field studies have investigated the volatility (Kuwayama et al., 2015; May et al., 2013a, 2013b, Li et al., 2016, Biswas et al., 2007; Grieshop et al., 2009) and mixing state (Tiitta et al., 2010, Liu et al., 2014, China et al., 2014, Willis et al., 2016) of traffic-emitted particles using various techniques, they have largely focused on measurements of sources or at fixed ambient location. To the best of our knowledge, no studies have been conducted to systematically explore the evolution of volatility and mixing state of near-road aerosols at different distances from the roadway under diverse environmental conditions.

We measured the evolution of a highway plume at different downwind distances under diverse environmental conditions under favorable wind directions during summer and winter field campaigns. Heating (using a thermodenuder) experimental data coupled with a mass transfer kinetics model were used to investigate particle volatility, and heating (V-TDMA: Volatility Tandem Differential Mobility Analyzer) and single particle data (SP2: Single Particle Soot Photometer) were used to explore mixing state of particles. The objectives of the study were to: (i) determine spatial distribution of aerosol volatility and mixing state in a near-road microenvironment, (ii) explore the influence of seasonality and ambient conditions on the phase-partitioning of near-road aerosols, and (iii) evaluate the representativeness of laboratory-derived POA volatility distributions from vehicle exhaust to explain real-world observations of aerosol volatility in a complex near-road microenvironment.

2. Methods

2.1. Measurement sites

Two month-long measurement campaigns were conducted at a site near Interstate 40 (I-40), outside Durham, North Carolina (35.865°N, 78.820°W) in Summer 2015 (June 1 –July 2) and Winter 2016 (January 18 – February 20). A map of the measurement site is shown in Figure S1. Detailed descriptions of the measurement site and campaigns are included in Saha et al. (2017a); they are only described briefly here. At the measurement location, I-40 has eight lanes and an annual average daily traffic volume of 140 to 145 thousand vehicles per day (4-6% of which are heavy-duty diesel vehicles (HDDV)). At our site, I-40 adjoins a low-traffic rural road running almost perpendicular to the highway, in-line with the dominant wind direction (southwest; 225º). This minor road allows us to study the evolution of the highway plume at different downwind distances. Measurements were collected at a fixed site trailer 10 m from the highway (continuous) and during downwind transects on the minor roadway at different downwind distances (10, 50, 100, 150, 220 m) from the highway (intermittent). Downwind transects measurements were performed on weekdays with the wind coming off of the highway consistently in summer (4 days) and winter (3 days). A mobile platform (van) was used for transects measurements. For a particular transect run, a sampling period at a downwind point was ~ 20 minutes; 4-5 downwind points were sampled consecutively. During sampling, the van engine was off to avoid self-contamination. A ‘full transect run’ took approximately 2 hours. Typically, three transect runs were completed per day: morning rush-hour (~7:00-9:00 am), mid-day (~12:30-2:30 pm) and evening rush hour (~4:30-6:30 pm).

To explore the spatial distribution of volatility and mixing state of particles, measurements collected during transect runs are the major focus of this paper.

2.2. Measurements

2.2.1 Thermodenuder (TD) experiments

Various configurations of heating (thermodenuder; TD) experimental approaches were applied to explore the volatility and mixing state of near-road aerosols. The methods applied here fall into two general categories: (i) heating of the polydisperse particle distribution (Huffman et al., 2008; Lee et al., 2010; Saha et al., 2017b), and (ii) heating of differential mobility analyzer- (DMA) selected monodisperse particles (volatility tandem DMA approach; V-TDMA) (Biswas et al., 2007; Kuhn et al., 2005; Tiitta et al., 2010). A custom-built, multi-tube thermodenuder (MT-TD) system was used for high time resolution volatility measurements. The MT-TD consists of four separate heated lines controlled by automated valves that can be switched in approximately 1 second, enabling quick alternation between four different set temperatures. While measuring the evaporation of a polydisperse distribution, the MT-TD was coupled with a Scanning Mobility Particle Sizer (SMPS, TSI Inc., 3010 CPC, 3081 DMA; scan time 2.5 minutes) to measure thermodenuded distributions (10-400 nm) after heating at 60, 90, 120, and 180 ºC with a residence time (Rt) of 30 s. All Rt values reported in this paper are volumetric residence time (volume/flow rate) at room temperature, unless otherwise stated. Dump flows were used to maintain constant flow in all lines during MT-TD operation. A full set of temperature scans required ~ 10 minutes. Another SMPS (3010 CPC, 3081 DMA; scan time 2.5 minutes) continuously measured particle size distributions (10-400 nm) at ambient temperature. In some transect runs, the V-TDMA configuration was used. In this approach, DMA size-selected monodisperse particles (25, 50, 100, 250 nm) were heated at different TD temperatures (60-180°C) with a Rt of 30 s and the thermodenuded distributions measured using an SMPS.

In the stationary roadside trailer, a temperature stepping TD (TS-TD) (Huffman et al., 2008; Saha et al., 2017b) was continuously operated at 4 temperature steps (60, 90, 120, 180°C; Rt = 30 s) upstream of an Aerosol Chemical Speciation Monitor (ACSM, Aerodyne Inc.; 75-650 nm) and SMPS (10-400 nm). In this configuration, instruments were alternated between the bypass (ambient) and TS-TD lines at 10 minutes intervals using an automated 3-way valve. TD/ACSM provides chemically resolved (organic, sulfate, nitrate, ammonium, and chloride) volatility data. Because TD data at different residence times provides additional constraints on the volatility parameter extraction process (Saha et al., 2015, 2017b), TD/SMPS data (10-400 nm) using the MT-TD setup were collected over a wide range of temperature and Rt conditions (T= 60, 90, 120 °C; Rt = 9, 13, 19, 30 s) during some of the summer campaign at the roadside trailer. An extra flow controller was used to vary Rt (Saha et al., 2015). In all measurements, a silica gel diffusion dryer was placed upstream of TD inlets and aerosol instruments to maintain relative humidity (RH) < 30-40%.

2.2.2 Single Particle Soot Photometer (SP2)

A SP2 (Droplet Measurement Technology; DMT Inc.) was deployed at the roadside trailer during the winter campaign to measure the size distribution and mixing state of BC. The SP2 uses a laser-induced incandescence (Nd:YAG laser; 1064 nm) technique (Stephens et al., 2003) to measure refractory BC mass (rBC) in individual particles. The rBC containing particles passing through the laser beam scatter laser light and at the same time absorb energy and are heated to their vaporization temperature and incandesce (McMeeking et al., 2011a; Moteki and Kondo, 2007; Shiraiwa et al., 2007; Stephens et al., 2003). The incandescent light is proportional to rBC core mass. The SP2 incandescence response was calibrated with DMA-selected dried fullerene soot particles. A calibration curve is derived from the SP2 incandescence response and mass of the calibration particles from the mobility diameter and assuming an effective density of 1.8 g cm^{-3}. The scattering detectors were calibrated using dried PSL (polystyrene latex spheres) particles by relating the detector response to the PSL sizes. Ambient particles were dried before introduction into the SP2.

2.2.3 Other supporting measurements

Measurements of traffic (volume, composition, speed) and meteorological data (ambient T, RH, wind speed, and direction) and various gaseous and particulate air pollutant concentrations were collected throughout the campaigns, and are discussed in detail in Saha et al. (2017a). A 10-meter meteorological tower recorded meteorological data at the roadside trailer location. An existing remote traffic microwave sensor (RTMS) maintained by the North Carolina Department of Transportation (NC-DOT) provided traffic data. Particle size distributions (SMPS; 10-400 nm), chemical composition (ACSM; 75-650 nm), BC (Photo-acoustic Extinctiometer; PAX-870, Droplet Measurement Technology; DMT Inc.), NO/NO_2 (2B Technology 401/410), CO_2 (Li-cor Li-820) were continuously measured from the roadside trailer. During transect runs, particle sizing (SMPS), NO, NO_2, BC, and CO_2 instruments from the trailer were placed in the transect van to collect these parameters at different distances from the highway. Particle size distribution (SMPS; 10-400 nm), NO/NO_2 (Ecotech 9841), BC (microAeth, AE51) were continuously monitored in an upwind stationary background site, located on the opposite side of I-40, approximately 400 m away from the highway.

2.3 Data reduction

Evaporation of particles at a particular TD operating condition (T, Rt) is described in terms of volume fraction remaining (VFR; for SMPS data) or mass fraction remaining (MFR; for ACSM data). VFR (MFR) is the ratio of volume (mass) concentration measured in heated line (C_{TD}) to that in unheated bypass line (C_{BP}). The size distribution for the heated, size-selected monodisperse particles (V-TDMA approach) was typically bimodal; one mode did not shrink upon heating (non-volatile mode) and the other did (volatile mode). VFR for the size-selected particles was estimated as $(D_{p,heated})^3/(D_{p,ambient})^3$, where $D_{p,ambient}$ is the mode diameter of the selected monodisperse particles at ambient temperature and $D_{p,heated}$ is the mode diameter of the volatile mode after heating at a particular temperature. Therefore, estimated VFR for the size-selected particles excludes the non-volatile population. Empirical particle loss correction factors (Saha et al., 2015), estimated as a function of TD operating conditions (T, Rt), were applied to the VFR from integrated SMPS volume and MFR from ACSM data. Because VFR for size-selected particles was calculated from the change in mode diameter, particle loss correction factors are not required in this calculation.

SP2 data were processed using the PSI (Paul Scherrer Institute) SP2 Toolkit. The rBC-containing particles are treated as an rBC core coated by a shell of other material. The size distribution of rBC-cores was derived based on the mass equivalent diameter (MED) of an rBC-core assuming a density of 1.8 cm^{-3}. The delay time between the peak of the incandescence and scattering signals is an indicator of the coating thickness (mixing state) (Moteki and Kondo, 2007), and was used to determine the number fraction of 'thinly coated' and 'thickly coated' rBC particles (McMeeking et al., 2011a; Shiraiwa et al., 2007; Subramanian et al., 2010).

2.4 Parameterizing volatility

An evaporation mass transfer kinetics model (Lee et al., 2011) was applied to infer particle volatility distributions by fitting TD data. The volatility distribution extraction framework used here is similar to that described in Saha et al. (2015). The resulting fit empirically describes the particle volatility distribution using a volatility basis set (VBS) framework (Donahue et al., 2006, 2012), where the material is lumped over a logarithmically spaced set of C* (effective saturation concentration) bins at a reference temperature of 25°C. A set of f_i describes the distribution of semi-volatile species (particle + gas phase) in selected C* bins under a gas-particle equilibrium and is usually known as volatility distribution. A 6 bin $\log_{10}$VBS with C* bin range of 10^{-4} μg m^{-3} to 10^{1} μg m^{-3} at 25 °C was selected to describe the particle volatility distribution empirically. Before the TD inlet, an initial gas-particle equilibrium at ambient temperature (summer 30°C, winter 5 °C) and campaign-average aerosol mass loading (C_{OA} ~5μg m^{-3}) were assumed. The Clausius-Clapyeron equation was applied to calculate temperature dependent C* (Saha et al. 2015).

The mass transfer kinetics model tracks particle and gas-phase concentrations of the surrogate species (represented by C* bins) as they pass through the TD. The TD-derived volatility distributions from kinetics model fits are sensitive to assumptions of enthalpy of vaporization (ΔH_{vap}) and evaporation coefficient (γ_e); these values are generally unknown *a priori* (Cappa and Jimenez, 2010). γ_e is often assumed to be in unity in fitting TD data (Grieshop et al., 2009; Li et al., 2016); however, recent studies reported a γ_e values between 0.01 and 1 for different aerosol systems (Cappa and Jimenez, 2010; Saha et al., 2017b; Saha and Grieshop, 2016; Saleh et al., 2013). Similarly, in literature, different ranges of ΔH_{vap} values are reported for different aerosol systems (Epstein et al., 2010; May et al., 2013c; Ranjan et al., 2012). TD data collected at varying (T, Rt) provides additional constraints on feasible γ_e and ΔH_{vap} values (Saha et al., 2015, 2017b; Saha and Grieshop, 2016). TD data over a wide range in (T, Rt) space were collected during the I-40 summer campaign at the near-road trailer, and are shown in Figure S2 (a-d). Following Saha et al. (2015, 2017b), we used this data set to optimize a set of γ_e and ΔH_{vap} values that best explain the evaporation observed in near-highway aerosols (see Figure S2e for details). A γ_e of 0.25 and ΔH_{vap} of 100 kj mol^{-1} provided the overall best fit for this data set. We adopted these estimated γ_e and ΔH_{vap} values for the near-highway aerosol system for further fitting of TD data from different distances from the highway across all seasons and sizes. Saha et al. (2017b) reported similar γ_e and ΔH_{vap} values for ambient TD data from two sites in the southeastern US under diverse conditions. Saleh et al. (2012) derived a γ_e value of 0.28-0.46 for ambient aerosols in Lebanon. Therefore, given the consistency in reported γ_e and ΔH_{vap} values across diverse settings (Saha et al., 2017b; Saleh et al., 2012), it is reasonable to use constant values for further fitting of TD data from the same site under different conditions. Other inputs to the mass transfer model include diffusion coefficient (D), surface tension (σ), molecular weight (MW) and density (ρ); the assumed values generally have a smaller influence on modeled evaporation in TDs (Cappa and Jimenez, 2010; Saha et al., 2015), and are approximated from literature (Table S1).

3. Results and discussion

3.1 Observed evaporations in TD with downwind distance

Figure 1 shows the measured VFR at 60°C as a function of distance from the highway. The particle volume fraction that evaporates at low and moderate TD temperature (e.g., 1-VFR at 60˚C) consists of semi-volatile species, presumably OA. VFR data are shown for different monodisperse particle sizes (e.g., 25, 50, 100, 250 nm), and for the integrated volume of polydisperse distributions. Results shows that the evaporation observed in a TD at 60°C decreases with downwind distance during transects in both seasons, which suggests a reduction in relative abundance of the semivolatile fraction in particles with distance. This reduction is especially pronounced over the ultrafine particle range (<100 nm). Two plausible reasons could contribute to this observation. First, a fraction of semi-volatile species in vehicle-emitted fresh particles may be evaporating during transport due to dilution-driven processes (Choi and Paulson, 2016; Robinson et al., 2007; Shrivastava et al., 2006). Second, since the concentration of vehicle-emitted particles decreases rapidly with distance from the highway, the relative proportion of background particles in the sampled aerosol (vehicle-emitted + background) increases with distance. If one assumes that background particles are less volatile than vehicle-emitted fresh particles, the relative abundance of the less-volatile material in the sampled aerosols will increase with distance. The influence of each factor cannot be isolated directly from TD measurements. However, the particle size distributions measured at background (upwind) and downwind locations from the highway (Figure S3) indicate that vehicle-emitted fresh particles are dominated by ultrafine particles (< 100 nm), while background particles are predominantly in a relatively larger mode. When polydisperse particles (10-400 nm) were heated at a moderate TD temperature (60°C), the changes in the larger size range (>100 nm) was observed to be minimal (Figure S4). Larger particles also do not show significant downwind gradients in evaporation upon heating at 60°C (Figure S4). Therefore, the observed downwind decrease in evaporation of ultrafine particles at 60°C is likely more influenced by the dilution-driven losses of semi-volatile species during downwind transport. It should be noted here that other processes, including coagulation, may influence the evolution of near-road aerosol size distribution. However, Zhang et al. (2004) reported that after the initial stage of dilution (tailpipe to on-road), the second phase (road-to-ambient) of aerosol size distribution evolution is dominated by condensation and dilution, while coagulation and deposition play minor roles. Therefore, we do not expect that coagulation is a dominant process in altering the physio-chemical properties of transported traffic particles within the near-road domain (10-200 m from the highway edge) where we conducted our measurements.

The general trends in evaporation at 60°C observed as a function of downwind distance were consistent between summer and winter (Figure 1). However, the evaporation observed in winter was slightly greater than that in summer, specifically closer to the highway and for smaller particles. This observation is consistent with that of Kuhn et al. (2005), who reported greater evaporation of near-road particles in winter at a particular TD temperature. Two possible factors may contribute to this inter-seasonal difference. First, the initial partitioning of SVOCs entering the TD is different; at colder temperatures, a higher fraction of semi-volatile materials is expected to partition into the particle-phase. An analysis of temperature effects on the partitioning of semi-volatile materials from vehicular emissions (see Figure S5) indicates that while 40-70% of semi-volatile emissions reside in the particle-phase under typical winter conditions (0-10°C), only 10-20% do so under summer conditions (20-30°C). This analysis used the gasoline POA volatility distribution from May et al. (2013a) and ΔH_{vap} from Ranjan et al. (2012) and considered a range of OA concentrations for a typical roadside environment (e.g., 0.5 to 5 $\mu g\ m^{-3}$). Second, the difference could be due inter-seasonal differences in emission properties (the volatility of emissions) and atmospheric dilution. The effect of these two effects cannot be isolated directly from TD observations, but application of an evaporation kinetics model can disentangle them to some extent. For example, during modeling, initial gas-particle equilibrium at ambient temperatures (winter ~5 °C, summer ~30°C) was assumed before the TD inlet, which will account for the ambient temperature effect on initial SVOC partitioning. Therefore, inter-seasonal differences in volatility of emissions (if any) should be reflected in the resulting fitted volatility distributions; these modelling results are discussed in Sec. 3.3.

Figure 2 shows the evaporation observed at a higher TD temperature (180°C). VFR of $PM_{0.4}$ (integrated volume between 10-400 nm) at 180 ˚C decreases with downwind distance. The particle volume fraction that does not evaporate at 180 ˚C will consist of BC, other refractory materials (e.g. metals, crustal materials) and/or extremely low volatile organics (ELVOCs; $C^{*}<10^{-3}\ \mu g\ m^{-3}$) (Donahue et al., 2012). ELVOCs in the atmosphere are formed from multiple sources and chemical processes (Ehn et al., 2014; Jokinen et al., 2015). Organic mass fraction remaining (OA MFR) at 180˚C measured in the roadside trailer (~10-20%) using the TD/ACSM likely provide an approximate estimate of ELVOCs (shown with green circles in Figure 2a, b). Similar values were measured during ambient TD measurements in urban background and rural sites in southeastern US (Saha et al., 2017b). Recent laboratory-derived POA volatility distributions suggest that the presence of ELVOCs in fresh traffic-emitted POA may not be significant (May et al., 2013a, 2013b). Therefore, as a first order approximation, ELVOCs measured in the near-highway environment are likely dominated by regional background aerosol, and thus a gradient downwind of the roadway is not expected. On the other hand, traffic emissions are a major contributor of BC in near-highway environments (Baldauf et al., 2008; Bond et al., 2013; DeWitt et al., 2015) and a rapid downwind decay of BC concentrations was observed in our site (Saha et al. 2017a), consistent with past studies (Karner et al., 2010).

The downwind gradients of VFR of $PM_{0.4}$ at 180°C correlate well with that of BC (Figure 2 a, b). A less sharp decay of BC during winter was also consistent with the gradient of VFR of $PM_{0.4}$ at 180°C in winter. Figure 2c shows a scatter plot of the BC fraction in PM versus VFR of $PM_{0.4}$ (at 180 ºC) after subtracting OA MFR (at 180ºC) measured at 10 m for the winter data set; a similar plot for the summer dataset is shown in Figure S6. These correlation analyses indicate that the observed downwind evolution of VFR at 180 °C is likely dictated by the BC component of the aerosol. The BC fraction in this analysis was estimated as the ratio of the PAX-measured BC to PM mass concentration from integrated volume-weighted SMPS size distributions with an estimated effective density of 1.5 g cm^{-3}. See Figure S7 for details on the estimation of effective density and comparison of submicron mass concentrations measured by SMPS and ACSM+PAX.

The diurnal profile of SP2-measured BC size distribution, shown in Figure S8, indicates that BC is strongly correlated with the diurnal profile of traffic volume, indicating vehicles are the major source of BC at this near-highway site. Figure 2d explores the contribution of BC to the thermodenuded SMPS size distribution at 180°C. In Figure 2d, to directly compare with the volume-weighted SMPS distribution, the mass-weighted BC size distribution was converted to a volume-weighted distribution by assuming a BC density of 1.8 g cm^{-3}. The BC distribution accounts for approximately 35% of the area under the thermodenuded particle size distribution at 180 °C (Figure 2d). The remaining approximately 65% of material should consist of different low-volatility species (e.g., ELVOCs and others). This is broadly consistent with the measured OA MFR at 180°C at the roadside trailer, which explained ~50% of measured VFR at 180°C at that location (Figure 2 a, b). Therefore, by combining measurements from different instruments and approaches, the analysis summarized in Fig.2 indicates that in a near-road environment, denuded particle volume at very high temperature (at 180 °C) can be approximated as ~ ELVOCs + BC, with a spatial distribution that is dictated by BC spatial trend (as a traffic tracer).

3.2 Mixing state of near-highway particles

Figure 3 examines the mixing state of near-highway particles using V-TDMA data. The heated size distributions of a size-selected monodisperse (at ambient temperature) aerosol at different TD temperature is referred to as a volatility spectra. Figure 3 shows the measured average volatility spectra of 25, 50, and 100 nm particles collected 10 m from the highway during summer; similar winter observations are shown in Figure S9. Heated monodisperse particles yield a bimodal size distribution; one mode (less volatile; LV mode) shows almost no change from its original diameter with heating, and the other mode (more volatile; MV mode) shrinks substantially with heating. Similar bimodal distributions have been observed in previous near-road studies (Biswas et al., 2007; Kuhn et al., 2005; Tiitta et al., 2010). The general trend was found to be consistent across seasons.

A large fraction of LV mode particles is expected to be fresh soot from traffic emissions. Figure 3 suggests that LV mode particles are externally mixed (e.g., soot and OA exist in different particles), because if they were internally mixed with semi-volatile organics or others compounds (i.e., were coated), the coating material would evaporate with heating and a substantial diameter reduction be observed. Several studies have shown that these LV mode particles are less hygroscopic using a V-

TDMA coupled with an H-TDMA system (Kuwata et al., 2007; Tiitta et al., 2010). The presence of externally mixed LV particles was observed for all sizes studied (25, 50, 100, and 250 nm). However, the LV mode was relatively less pronounced for smaller sizes (e.g., 25 nm) compared to larger particles (e.g., 100 nm). The SP2-measured BC number size distribution peaked around 100-130 nm (see Figure 2d and Figure S8c), consistent with this observation. Kuhn et al. (2005) and Biswas et al. (2007) also reported that the less/non-volatile fraction of near-road aerosols increased with size within the size range studied (20-120 nm) in near-road V-TDMA measurements in California.

Figure 4 explores the mixing state of near-highway BC particles using the SP2 lag-time approach (Moteki and Kondo, 2007; Schwarz et al., 2006; Shiraiwa et al., 2007; Subramanian et al., 2010). The delay time between the occurrence of scattering and incandescence peaks observed in the SP2 can be used as an indicator of relative coating thickness ($\Delta\tau = \tau_{incandescence} - \tau_{scattering}$ = time to 'boil off' coating) (McMeeking et al., 2011a; Moteki and Kondo, 2007). Figure 4 shows the frequency distributions (histograms) of delay time (Δτ). Following McMeeking et al. (2011a), the entire ensemble of refractory BC-containing particles with scattering responses within detection range was considered in this analysis. Measurements are stratified by wind direction to separate those measured during wind events coming off of the highway (southwesterly; 225±45º) to the monitoring site and the opposite wind direction (northeasterly; 45±45º). Two distinct peaks near Δτ ~0.5 µs and ~3.5 µs appear in the Δτ frequency distribution. We use this to classify BC particles into two types using a threshold Δτ of 2 µs: thinly coated BC ($\Delta\tau < 2\mu s$) and thickly coated BC ($\Delta\tau > 2\mu s$). The threshold criterion is based on the observed minimum in the bimodal frequency distribution of Δτ (McMeeking et al., 2011a; Moteki and Kondo, 2007).

Figure 4 shows that a large fraction (up to 80%) of refractory BC (rBC) containing particles at this near-highway site are thinly coated (externally mixed), and are likely fresh soot particles from traffic emissions. The observed relative proportion of thinly coated (fresh) particles increases when the wind comes off of the highway to the monitoring station (southwesterly wind) (see Figure 4), suggesting that the local source (I-40 traffic) was the main contributor to this fraction. Using the data collected with the wind coming off of the highway, Figure S10 shows the linkage among the diurnal variation of Δτ frequency distributions, BC size distributions, and thermodenuded SMPS size distribution at 180°C. The thinly-coated fraction was found to be slightly higher in the midday and morning compared to the evening. This trend correlates with the diurnal variation of heavy-duty vehicle (HDV) fraction (indicated in inset of Figure S10), suggesting that HDV are the dominant contributor to the observed fresh (thinly-coated) BC fraction. The thickly coated fraction is likely contributed by regional background aged BC particles. However, approximately 10% of fresh BC from vehicular emissions could be thickly coated as reported by Willis et al. (2016). With an opposite wind (northeasterly), a minimum direct influence from I-40 traffic is expected at our monitoring location. The observed thickly coated fraction at that wind condition went up to 41%. This range of values are consistent with past studies, For example, a thickly coated rBC fraction of approximately 30-40% is reported in previous measurements in diverse urban environments (McMeeking et al., 2011a; Shiraiwa et al., 2007; Subramanian et al., 2010).

The substantial presence of thinly-coated (fresh) rBC suggested by the SP2 data (Figure 4) is consistent with our independently measured V-TDMA observations of externally-mixed characteristics for LV mode particles (Figure 3, Figure

S9). These observations are also in agreement with several recent studies that examined the mixing state of rBC from traffic emissions using a range of techniques (China et al., 2014; Kuwata et al., 2009; Liu et al., 2014; McMeeking et al., 2011b; Willis et al., 2016). Willis et al. (2016) reported approximately 90% of rBC mass resides in rBC-rich particles using Soot Photometers – Aerosol Mass Spectrometer (SP-AMS) measurements of traffic emissions in an urban setting, whereas the remaining 10% were mixed with hydrocarbon-like OA (HOA). China et al. (2014) reported ~72 % of soot particles from vehicle exhaust are barely or thinly coated using microscopic imaging technique. Traffic-dominated rBC particles were reported to be uncoated or very thinly coated by Laborde et al. (2013) and Liu et al. (2014) using SP2 measurements in urban environments.

Figure 5 compares similar V-TDMA measurements of 100 nm particles at different distances from the highway to examine the evolution of mixing state of particles with downwind transport. The overall concentration of both LV and MV mode particles rapidly decreases with distance due to dilution and mixing with cleaner background air. However, LV mode particles (e.g., BC) remain mostly externally mixed at 220 m downwind distance. This result indicates that there is minimal change in the mixing state in traffic-emitted particles between the near-road (~10 m) and far-road (~220 m) locations. Specifically, the proportion of internally versus externally mixed particles doesn't appear to change, nor is there evidence of substantial coating on externally mixed 'non-volatile' particles. Evolution of BC mixing state is typically observed in the atmosphere with photochemical aging; externally mixed BC particles (thinly coated) become progressively internally mixed (thickly coated) via formation of condensable vapors via photochemical processes followed by condensation on BC. Timescales on the order of an hour are typically required to observe a significant change in BC coating (Adachi and Buseck, 2013; McMeeking et al., 2011a; Shiraiwa et al., 2007; Subramanian et al., 2010). Since transport times of particles at 220 m downwind from the highway are on the order of a few seconds to minutes, it is not surprising to observe no significant change in mixing state of traffic-emitted particles (e.g., BC) within this short distance.

3.3 Inferred volatility distributions from TD data

This section discusses TD-derived volatility distributions at different distances from the highway to provide insight into the evolution of volatility of traffic emitted particles and provide parameterizations to explain phase-partitioning of near-road particles in similar microenvironments and laboratory observations. For this, we focus on the measured evaporation of ultrafine particles (25, 50, and 100 nm) at 10 and 220 m distances. Figure 6 shows measured and modeled thermograms (plots of VFR versus TD temperature) for TD measurements of varying particle sizes collected at different distances and seasons. At a particular TD temperature, smaller particles evaporate more than larger size particles (Figure 6). Size or composition (volatility distribution) may contribute to differential evaporation observed for different size particles (Saleh et al. 2011); both factors were taken into account during evaporation kinetics modeling following the framework described in Saha et al. (2015). The evaporation kinetics model tracks changes in diameter as aerosol with prescribed properties pass through the TD at a particular operating condition (T, Rt), as described in Sec 2.4; model VFR was estimated based on predicted change in particle diameter.

In our fitting, we solved for particle volatility distributions (particle-phase distribution;$\{x\}_i$) via least-squares fitting of modeled and measured VFR. Fitted distributions are listed in Table S2 and model lines in Figure 6 are shown using these best-fit distributions. Our fitting results (Figure 6) show that at a particular downwind-point, a single volatility distribution can explain the observed evaporations for different sized particles, suggesting particles within this size range have a consistent volatility distribution or chemical signature. We also report f_i distributions (Table 1) after converting our TD-derived particle-phase distributions (x_i) to total (gas+particle) distributions (f_i) under a gas-particle equilibrium conditions and assuming a typical near-road OA loading of ~ 5 μg m^{-3} (see SI Sec. S3 for details).

Figure 7 shows simplified representations of particle volatility distributions at roadside (10 m) and downwind (220 m) locations across summer and winter seasons. In this figure, distributions of particle-phase material are shown in two broad volatility categories: extremely-low+low volatility (ELVOC+LVOC) (C^* bins ≤ 0.1 μg m^{-3}) and semi-volatile (SVOC) (C^* bins ≥ 1 μg m^{-3}) (Donahue et al., 2012). A laboratory-derived POA volatility distribution of gasoline vehicle exhaust by May et al. (2013a) (derived from chromatographic analyses of filter samples) is also shown under a typical near-road aerosol loading ($C_{OA} = 5$ μg m^{-3}). The volatility distributions shown in Figure 7 and also reported in Table 1 and Table S2 are at a reference temperature of 25°C, which allows a convenient side-by-side comparison across seasons and with previous studies. The gasoline POA distribution by May et al. (2013a) places ~45% of OA in the SVOC bins under this condition. Our TD-derived results show that overall volatility of near-road particles is lower than laboratory-derived POA distribution, varies across seasons, and decreases with distance. The extracted volatility distributions of near-road particles is a mixture of traffic-emitted POA and background particles. Therefore, it is not expected that the overall volatility of near-road particles would be the same as that of vehicle POA. In Sec. 3.4, we use our spatial measurements of near-road aerosol (traffic+background) volatility to assess how/whether this laboratory-derived POA distribution can be used to represent the overall near-road volatility under real-world conditions.

Figure 7 indicates that the overall volatility of near-road aerosols decreases with distance from the highway in both seasons. For example, the TD-derived distributions apportion approximately 20-30% and 10% of particle-phase mass as SVOC at 10 and 220 m, respectively; consistent with dilution-driven evaporation of SVOCs and/or mixing with the background particles. When a volatility comparison is made at a common temperature of 25 °C (Figure 7), the particle volatility was found to be slightly higher for the winter data set than summer, especially closer to the highway. The extent of dilution and temperature of dilution air dictate the overall partitioning of semi-volatile emissions. Atmospheric dilution was substantially lower in winter at our site (and generally) due to more stable atmospheric conditions under colder weather (Saha et al., 2017a). Therefore, when comparing particle volatility at the same temperature, lower dilution during winter likely explains the observed higher SVOCs fraction.

The volatility comparison in Figure 7 is shown at a reference temperature of 25ºC; actual partitioning will vary with ambient temperature. Under a particular C_{OA} loading (atmospheric dilution), it is expected that a higher fraction of semi-volatile material partitions into the particle-phase at colder temperatures. Figure S11, an alternate version of Figure 7, shows the volatility comparison at campaign-average ambient temperatures of ~5 and ~30º C in winter and summer, respectively. After accounting for seasonal temperature difference, Figure S11 indicates that the particle-phase SVOCs fraction are approximately 2.5 times higher in winter (45%) than summer (18%) at the roadside location (10 m). During winter, a higher fraction of semi-volatile particles may form via homogeneous nucleation during a rapid cooling of vehicle exhaust under a lower ambient temperature (Du and Yu, 2006; Kittelson et al., 2006; Kittelson and Kraft, 2014). This fact was supported by our observed three-fold increase in ultrafine particle and also HOA emission factors during winter in compared to summer, discussed in Saha et al. (2017a). This result implies that human exposure to semi-volatile particles at a near-road location could vary substantially across seasons and would be more extreme in colder weather.

3.4 Evaluation of laboratory-derived POA distributions to explain real-world partitioning

Particle mass concentrations measured next to a highway are a mixture of a traffic contribution and background particles (road-side PM = traffic+ background). It can be reasonably hypothesized that the volatility distribution of road-side particles at a particular downwind location is a superposition of that from background particles and traffic-contributed particles at that location (Eq. 1). One can test this hypothesis if the volatility distributions of different populations of particles (road-side, background, traffic) are known. Vehicle-emitted POA volatility distributions have been derived in laboratory studies (May et al., 2013a, 2013b) of a relatively small number of vehicles in controlled laboratory tests; they have also recently been measured in a traffic tunnel study (Li et al., 2016). Here, we used our spatial measurements of particle volatility distributions along with a laboratory-derived POA distribution from May et al. (2013a) to assess our ability to represent the volatility of POA from the overall traffic fleet in a complex near-road microenvironment.

$$C_{\text{OA, roadside}} \times x_{\text{i, roadside}} = C_{\text{OA, traffic}} \times x_{\text{i, traffic}} + C_{\text{OA, background}} \times x_{\text{i, background}} \qquad \text{[Eq.1]}$$

Where, C_{OA} (µg m^{-3}) is the organic aerosol (OA) mass concentrations, and x_i is the distribution of OA mass concentrations at different volatility bins, following volatility basis set (VBS) approach (Donahue et al, 2006).

To test Eq.1, we conducted an analysis using an example data set from a morning transect on June 12, 2015 (summer), with the wind consistently coming off of the highway; the details on analysis are given in SI, Sec. S4. Analysis results are shown in Fig.8. The contribution of traffic particles in road-side measurements was estimated as the difference between concentrations measured at roadside (downwind) and upwind background location. Figure 8a shows the measured upwind (background) and downwind organic aerosol (OA) mass concentrations as a function of distances from the highway. It should be noted here that approximate estimates of OA mass concentrations in Fig. 8a are calculated from integrated volume from SMPS measurements and an estimated effective density of 1.5 g cm^{-3} (Figure S7) and subtracting the contribution of BC (as a function of distance), nitrate and sulfate aerosols (measured by an ACSM at the near-road fixed site trailer).

Figure 8b compares our measured road-side volatility distribution (at 10 m) with a distribution reconstructed from traffic and background distributions. Distributions of particle-phase-only OA concentrations are shown. In this analysis, the volatility distribution of POA emissions from gasoline vehicle exhaust from May et al. (2013a) (Table 1) is assumed to be representative of the overall traffic-emitted OA. Since we did not measure particle volatility at our upwind background site, we assume that the volatility distribution measured at our far-from-road downwind location (220 m) is a representative distribution for background particles. This is a reasonable approximation as particle concentrations approach background levels within 200-300 m from the highway (Saha et al., 2017a). It should be noted that this ‘background’ OA contains a non-negligible (~25%) contribution from traffic emissions (Fig. 8a), and so likely has a slightly greater contribution from higher-volatility components than what would be measured in an actual ‘background’ location. Our measured distributions from the summer campaign (Table 1) were used to be consistent with the OA concentration measurements in this particular example. Overall, a good agreement was found between the measured distribution at 10 m downwind and superimposed distribution of (background+ traffic POA) (Figure 8b). In particular, the contribution from more volatile materials ($C^* = 1$ and 10 µg m^{-3}) from traffic POA is required to explain the greater contribution from these more volatile species at 10 m vs. 220 m from the roadway. Therefore, this analysis indicates that laboratory-derived volatility distribution from May et al. (2013a) can do a reasonably good job in explaining the observed partitioning of vehicle emissions in a complex near-road environment. In addition to the analysis in Fig.8b, a similar analysis is shown in Figure S12 using the ‘coarse’ tracer m/z based factor analysis approach to decompose OA mass spectra (Ng et al., 2011), where the Hydrocarbon-like OA (HOA) factor is assumed to represent traffic-sourced OA and oxygenated-OA (OOA) background-OA. The details of this analysis are discussed in SI, Sec. S5. While this simplified ‘superposition’ analysis suggests that our data are able to capture the influences of near-road evolution on emissions, further measurements and modelling work are needed to represent these dynamic processes.

4. Conclusions and Implications

Field experiments were conducted across two seasons in an effort to explore the evolution of volatility and mixing state of near-road particles within a few hundred meters downwind of a highway. The spatial distributions of the volatility of near-road aerosols varied with distance from the highway and season. The overall volatility of near-road particles decreases with distance from the roadway. For example, at a reference temperature of 25 ºC, while approximately 20-30% of particle mass was classified as semi-volatile (SVOCs; $C^* \geq 1 \mu g\ m^{-3}$) 10 m from the roadway, only ~10% of particle mass was attributed to semi-volatiles at 220 m. The decrease of the semi-volatile fraction in particle-phase with downwind distance is likely due to dilution-driven evaporation of SVOCs as fresh vehicle-emitted particles are transported downwind and/or mix with background particles. The relative abundance of semi-volatile material in the particle-phase increased during winter, especially closer to the highway, reflecting the effect of temperature on semi-volatile partitioning. The non-volatile fraction in roadside aerosols appeared to be mostly externally mixed, and their mixing state showed minimal change within a few hundred meters from the highway.

This research has several important implications for measurement and modeling of emissions and exposure to ultrafine particles (UFPs) in a near-road microenvironment and its regulation. First, the measured particle number (PN) concentrations in near-road settings are dominated by UFPs. In a companion paper (Saha et al. 2017a), we showed that UFP number emission factors are substantially higher, and dispersion slower, during winter, indicating human exposure to UFPs would be significantly higher in colder conditions. This paper shows that a significant fraction of UFPs is semi-volatile in nature, and hence a larger portion of semi-volatile materials likely exist in particle-phase in colder conditions. Current European vehicle particle number emission standards use measurements of thermally treated exhaust that strips the semi-volatile particle components to constrain variability between measurement approaches (Wang et al., 2017). As a result, this regulatory measurement likely does not address the seasonally- and spatially-varying real-world particle number concentrations and compositions to which people are exposed. Several recent toxicology studies (Biswas et al., 2009; Keebaugh et al., 2015) reported that the semi-volatile species in traffic-sourced particles could be more toxic than less volatile components. Therefore, our observed seasonal variation in UFPs emission factors and semi-volatile components in the particle-phase suggest that human exposure to UFPs and its toxicity in a near-road microenvironment could vary with seasons and environmental conditions and would be more extreme in colder weather. The elevated fraction of semi-volatile materials in roadside particles and their potential higher toxicity suggest that an equivalent amount of exposure (concentration × duration) to roadside versus background particles could have significantly different health impacts. However, the toxicity of different volatility and size classes of PM is not well established in the current literature. For example, Cho et al. (2009) reported no significant difference in the overall toxicity end points for PM samples collected at 20 m and 275 m from an interstate highway. Further research is needed to better understand toxicity and health impacts of different volatility and size classes of PM from different sources and environmental conditions. Second, our finding of externally mixed near-road particles suggests that exposure to BC and OA containing particles could be different across seasons. For example, OA containing particles will be more dynamic under changing ambient conditions. Environmental conditions (temperature, atmospheric dilution) will influence the gas-particle partitioning of SVOCs, thus exposure to condensed- versus vapor-phase SVOC under changing ambient conditions. On the other hand, exposure to BC would be less influenced by changing ambient conditions. Finally, the volatility distributions and mixing state characteristics of near-road particles derived here can be used to examine the representativeness of laboratory derived results in complex real-world scenario (as shown via an example in this paper) and to improve the representation of traffic-sourced aerosols in air quality, exposure assessment and chemical transport models.

Acknowledgements

We thank Sue Kimbrough, Rich Baldauf and Richard Snow of the US EPA Office of Research and Development, Research Triangle Park (RTP), NC for help and support with establishing the roadside trailer facility for this study. We thank Steve Weiandt (Atlantic Investment Management) for providing access and support with establishing the background site for this study. We thank Nagui Rouphail and his research group (NCSU) and NC-DOT for the traffic data used in this paper.

Funding was provided by the Health Effects Institute (HEI) under RFA 13-1. Contents of this paper are solely the responsibility of the authors and do not necessarily represent the official views of HEI, and no official endorsement should be inferred.

References

Adachi, K. and Buseck, P. R.: Changes of ns-soot mixing states and shapes in an urban area during CalNex, J. Geophys. Res. Atmospheres, 118(9), 3723–3730, doi:10.1002/jgrd.50321, 2013.

Baldauf, R., Thoma, E., Hays, M., Shores, R., Kinsey, J., Gullett, B., Kimbrough, S., Isakov, V., Long, T., Snow, R., Khlystov, A., Weinstein, J., Chen, F.-L., Seila, R., Olson, D., Gilmour, I., Cho, S.-H., Watkins, N., Rowley, P. and Bang, J.: Traffic and Meteorological Impacts on Near-Road Air Quality: Summary of Methods and Trends from the Raleigh Near-Road Study, J. Air Waste Manag. Assoc., 58(7), 865–878, doi:10.3155/1047-3289.58.7.865, 2008.

Biswas, S., Ntziachristos, L., Moore, K. F. and Sioutas, C.: Particle volatility in the vicinity of a freeway with heavy-duty diesel traffic, Atmos. Environ., 41(16), 3479–3493, doi:10.1016/j.atmosenv.2006.11.059, 2007.

Bond, T. C., Doherty, S. J., Fahey, D. W., Forster, P. M., Berntsen, T., DeAngelo, B. J., Flanner, M. G., Ghan, S., Kärcher, B., Koch, D., Kinne, S., Kondo, Y., Quinn, P. K., Sarofim, M. C., Schultz, M. G., Schulz, M., Venkataraman, C., Zhang, H., Zhang, S., Bellouin, N., Guttikunda, S. K., Hopke, P. K., Jacobson, M. Z., Kaiser, J. W., Klimont, Z., Lohmann, U., Schwarz, J. P., Shindell, D., Storelvmo, T., Warren, S. G. and Zender, C. S.: Bounding the role of black carbon in the climate system: A scientific assessment, J. Geophys. Res. Atmospheres, 118(11), 5380–5552, doi:10.1002/jgrd.50171, 2013.

Broday, D. M. and Rosenzweig, R.: Deposition of fractal-like soot aggregates in the human respiratory tract, J. Aerosol Sci., 42(6), 372–386, doi:10.1016/j.jaerosci.2011.03.001, 2011.

Canagaratna, M. R., Onasch, T. B., Wood, E. C., Herndon, S. C., Jayne, J. T., Cross, E. S., Miake-Lye, R. C., Kolb, C. E. and Worsnop, D. R.: Evolution of Vehicle Exhaust Particles in the Atmosphere, J. Air Waste Manag. Assoc., 60(10), 1192–1203, doi:10.3155/1047-3289.60.10.1192, 2010.

Cappa, C. D. and Jimenez, J. L.: Quantitative estimates of the volatility of ambient organic aerosol, Atmos Chem Phys, 10(12), 5409–5424, doi:10.5194/acp-10-5409-2010, 2010.

Cappa, C. D., Onasch, T. B., Massoli, P., Worsnop, D. R., Bates, T. S., Cross, E. S., Davidovits, P., Hakala, J., Hayden, K. L., Jobson, B. T., Kolesar, K. R., Lack, D. A., Lerner, B. M., Li, S.-M., Mellon, D., Nuaaman, I., Olfert, J. S., Petäjä, T., Quinn, P. K., Song, C., Subramanian, R., Williams, E. J. and Zaveri, R. A.: Radiative Absorption Enhancements Due to the Mixing State of Atmospheric Black Carbon, Science, 337(6098), 1078–1081, doi:10.1126/science.1223447, 2012.

China, S., Salvadori, N. and Mazzoleni, C.: Effect of Traffic and Driving Characteristics on Morphology of Atmospheric Soot Particles at Freeway On-Ramps, Environ. Sci. Technol., 48(6), 3128–3135, doi:10.1021/es405178n, 2014.

Choi, W. and Paulson, S. E.: Closing the ultrafine particle number concentration budget at road-to-ambient scale: Implications for particle dynamics, Aerosol Sci. Technol., 50(5), 448–461, doi:10.1080/02786826.2016.1155104, 2016.

Dallmann, T. R. and Harley, R. A.: Evaluation of mobile source emission trends in the United States, J. Geophys. Res. Atmospheres, 115(D14), D14305, doi:10.1029/2010JD013862, 2010.

Dallmann, T. R., Onasch, T. B., Kirchstetter, T. W., Worton, D. R., Fortner, E. C., Herndon, S. C., Wood, E. C., Franklin, J. P., Worsnop, D. R., Goldstein, A. H. and Harley, R. A.: Characterization of particulate matter emissions from on-road gasoline and diesel vehicles using a soot particle aerosol mass spectrometer, Atmos Chem Phys, 14(14), 7585–7599, doi:10.5194/acp-14-7585-2014, 2014.

DeCarlo, P. F., Slowik, J. G., Worsnop, D. R., Davidovits, P. and Jimenez, J. L.: Particle Morphology and Density Characterization by Combined Mobility and Aerodynamic Diameter Measurements. Part 1: Theory, Aerosol Sci. Technol., 38(12), 1185–1205, doi:10.1080/027868290903907, 2004.

DeWitt, H. L., Hellebust, S., Temime-Roussel, B., Ravier, S., Polo, L., Jacob, V., Buisson, C., Charron, A., André, M., Pasquier, A., Besombes, J. L., Jaffrezo, J. L., Wortham, H. and Marchand, N.: Near-highway aerosol and gas-phase measurements in a high-diesel environment, Atmos Chem Phys, 15(8), 4373–4387, doi:10.5194/acp-15-4373-2015, 2015.

Donahue, N. M., Robinson, A. L., Stanier, C. O. and Pandis, S. N.: Coupled Partitioning, Dilution, and Chemical Aging of Semivolatile Organics, Environ. Sci. Technol., 40(8), 2635–2643, doi:10.1021/es052297c, 2006.

Donahue, N. M., Kroll, J. H., Pandis, S. N. and Robinson, A. L.: A two-dimensional volatility basis set – Part 2: Diagnostics of organic-aerosol evolution, Atmos Chem Phys, 12(2), 615–634, doi:10.5194/acp-12-615-2012, 2012.

Ehn, M., Thornton, J. A., Kleist, E., Sipilä, M., Junninen, H., Pullinen, I., Springer, M., Rubach, F., Tillmann, R., Lee, B., Lopez-Hilfiker, F., Andres, S., Acir, I.-H., Rissanen, M., Jokinen, T., Schobesberger, S., Kangasluoma, J., Kontkanen, J., Nieminen, T., Kurtén, T., Nielsen, L. B., Jørgensen, S., Kjaergaard, H. G., Canagaratna, M., Maso, M. D., Berndt, T., Petäjä, T., Wahner, A., Kerminen, V.-M., Kulmala, M., Worsnop, D. R., Wildt, J. and Mentel, T. F.: A large source of low-volatility secondary organic aerosol, Nature, 506(7489), 476–479, doi:10.1038/nature13032, 2014.

Epstein, S. A., Riipinen, I. and Donahue, N. M.: A Semiempirical Correlation between Enthalpy of Vaporization and Saturation Concentration for Organic Aerosol, Environ. Sci. Technol., 44(2), 743–748, doi:10.1021/es902497z, 2010.

Fraser, M. P., Cass, G. R. and Simoneit, B. R. T.: Particulate organic compounds emitted from motor vehicle exhaust and in the urban atmosphere, Atmos. Environ., 33(17), 2715–2724, doi:10.1016/S1352-2310(98)00311-2, 1999.

Grieshop, A. P., Miracolo, M. A., Donahue, N. M. and Robinson, A. L.: Constraining the Volatility Distribution and Gas-Particle Partitioning of Combustion Aerosols Using Isothermal Dilution and Thermodenuder Measurements, Environ. Sci. Technol., 43(13), 4750–4756, doi:10.1021/es8032378, 2009.

Health Effects Institute: Traffic-Related Air Pollution: A Critical Review of the Literature on Emissions, Exposure, and Health Effects, Health Eff. Inst. [online] Available from: https://www.healtheffects.org/publication/traffic-related-air-pollution-critical-review-literature-emissions-exposure-and-health (Accessed 4 January 2017), 2010.

Hoek, G., Boogaard, H., Knol, A., de Hartog, J., Slottje, P., Ayres, J. G., Borm, P., Brunekreef, B., Donaldson, K., Forastiere, F., Holgate, S., Kreyling, W. G., Nemery, B., Pekkanen, J., Stone, V., Wichmann, H.-E. and van der Sluijs, J.: Concentration Response Functions for Ultrafine Particles and All-Cause Mortality and Hospital Admissions: Results of a European Expert Panel Elicitation, Environ. Sci. Technol., 44(1), 476–482, doi:10.1021/es9021393, 2009.

Huffman, J. A., Ziemann, P. J., Jayne, J. T., Worsnop, D. R. and Jimenez, J. L.: Development and Characterization of a Fast-Stepping/Scanning Thermodenuder for Chemically-Resolved Aerosol Volatility Measurements, Aerosol Sci. Technol., 42(5), 395–407, doi:10.1080/02786820802104981, 2008.

Jokinen, T., Berndt, T., Makkonen, R., Kerminen, V.-M., Junninen, H., Paasonen, P., Stratmann, F., Herrmann, H., Guenther, A. B., Worsnop, D. R., Kulmala, M., Ehn, M. and Sipilä, M.: Production of extremely low volatile organic compounds from biogenic emissions: Measured yields and atmospheric implications, Proc. Natl. Acad. Sci., 112(23), 7123–7128, doi:10.1073/pnas.1423977112, 2015.

Karner, A. A., Eisinger, D. S. and Niemeier, D. A.: Near-Roadway Air Quality: Synthesizing the Findings from Real-World Data, Environ. Sci. Technol., 44(14), 5334–5344, doi:10.1021/es100008x, 2010.

Kleeman, M. J., Schauer, J. J. and Cass, G. R.: Size and Composition Distribution of Fine Particulate Matter Emitted from Motor Vehicles, Environ. Sci. Technol., 34(7), 1132–1142, doi:10.1021/es981276y, 2000.

Kuhn, T., Biswas, S. and Sioutas, C.: Diurnal and seasonal characteristics of particle volatility and chemical composition in the vicinity of a light-duty vehicle freeway, Atmos. Environ., 39(37), 7154–7166, doi:10.1016/j.atmosenv.2005.08.025, 2005.

Kumar, P., Ketzel, M., Vardoulakis, S., Pirjola, L. and Britter, R.: Dynamics and dispersion modelling of nanoparticles from road traffic in the urban atmospheric environment—A review, J. Aerosol Sci., 42(9), 580–603, doi:10.1016/j.jaerosci.2011.06.001, 2011.

Kuwata, M., Kondo, Y., Mochida, M., Takegawa, N. and Kawamura, K.: Dependence of CCN activity of less volatile particles on the amount of coating observed in Tokyo, J. Geophys. Res. Atmospheres, 112(D11), D11207, doi:10.1029/2006JD007758, 2007.

Kuwata, M., Kondo, Y. and Takegawa, N.: Critical condensed mass for activation of black carbon as cloud condensation nuclei in Tokyo, J. Geophys. Res. Atmospheres, 114(D20), D20202, doi:10.1029/2009JD012086, 2009.

Laborde, M., Crippa, M., Tritscher, T., Jurányi, Z., Decarlo, P. F., Temime-Roussel, B., Marchand, N., Eckhardt, S., Stohl, A., Baltensperger, U., Prévôt, A. S. H., Weingartner, E. and Gysel, M.: Black carbon physical properties and mixing state in the European megacity Paris, Atmos Chem Phys, 13(11), 5831–5856, doi:10.5194/acp-13-5831-2013, 2013.

Lee, B. H., Kostenidou, E., Hildebrandt, L., Riipinen, I., Engelhart, G. J., Mohr, C., DeCarlo, P. F., Mihalopoulos, N., Prevot, A. S. H., Baltensperger, U. and Pandis, S. N.: Measurement of the ambient organic aerosol volatility distribution: application during the Finokalia Aerosol Measurement Experiment (FAME-2008), Atmos Chem Phys, 10(24), 12149–12160, doi:10.5194/acp-10-12149-2010, 2010.

Lee, B.-H., Pierce, J. R., Engelhart, G. J. and Pandis, S. N.: Volatility of secondary organic aerosol from the ozonolysis of monoterpenes, Atmos. Environ., 45(14), 2443–2452, doi:10.1016/j.atmosenv.2011.02.004, 2011.

Li, X., Dallmann, T. R., May, A. A., Tkacik, D. S., Lambe, A. T., Jayne, J. T., Croteau, P. L. and Presto, A. A.: Gas-Particle Partitioning of Vehicle Emitted Primary Organic Aerosol Measured in a Traffic Tunnel, Environ. Sci. Technol., 50(22), 12146–12155, doi:10.1021/acs.est.6b01666, 2016.

Liu, D., Allan, J. D., Young, D. E., Coe, H., Beddows, D., Fleming, Z. L., Flynn, M. J., Gallagher, M. W., Harrison, R. M., Lee, J., Prevot, A. S. H., Taylor, J. W., Yin, J., Williams, P. I. and Zotter, P.: Size distribution, mixing state and source apportionment of black carbon aerosol in London during wintertime, Atmos Chem Phys, 14(18), 10061–10084, doi:10.5194/acp-14-10061-2014, 2014.

Maricq, M. M. and Xu, N.: The effective density and fractal dimension of soot particles from premixed flames and motor vehicle exhaust, J. Aerosol Sci., 35(10), 1251–1274, doi:10.1016/j.jaerosci.2004.05.002, 2004.

Matti Maricq, M.: Chemical characterization of particulate emissions from diesel engines: A review, J. Aerosol Sci., 38(11), 1079–1118, doi:10.1016/j.jaerosci.2007.08.001, 2007.

May, A. A., Presto, A. A., Hennigan, C. J., Nguyen, N. T., Gordon, T. D. and Robinson, A. L.: Gas-particle partitioning of primary organic aerosol emissions: (1) Gasoline vehicle exhaust, Atmos. Environ., 77, 128–139, doi:10.1016/j.atmosenv.2013.04.060, 2013a.

May, A. A., Presto, A. A., Hennigan, C. J., Nguyen, N. T., Gordon, T. D. and Robinson, A. L.: Gas-Particle Partitioning of Primary Organic Aerosol Emissions: (2) Diesel Vehicles, Environ. Sci. Technol., 47(15), 8288–8296, doi:10.1021/es400782j, 2013b.

May, A. A., Levin, E. J. T., Hennigan, C. J., Riipinen, I., Lee, T., Collett, J. L., Jimenez, J. L., Kreidenweis, S. M. and Robinson, A. L.: Gas-particle partitioning of primary organic aerosol emissions: 3. Biomass burning, J. Geophys. Res. Atmospheres, 118(19), 2013JD020286, doi:10.1002/jgrd.50828, 2013c.

McMeeking, G. R., Morgan, W. T., Flynn, M., Highwood, E. J., Turnbull, K., Haywood, J. and Coe, H.: Black carbon aerosol mixing state, organic aerosols and aerosol optical properties over the United Kingdom, Atmos Chem Phys, 11(17), 9037–9052, doi:10.5194/acp-11-9037-2011, 2011a.

McMeeking, G. R., Good, N., Petters, M. D., McFiggans, G. and Coe, H.: Influences on the fraction of hydrophobic and hydrophilic black carbon in the atmosphere, Atmos Chem Phys, 11(10), 5099–5112, doi:10.5194/acp-11-5099-2011, 2011b.

Moteki, N. and Kondo, Y.: Effects of Mixing State on Black Carbon Measurements by Laser-Induced Incandescence, Aerosol Sci. Technol., 41(4), 398–417, doi:10.1080/02786820701199728, 2007.

Ng, N. L., Canagaratna, M. R., Jimenez, J. L., Zhang, Q., Ulbrich, I. M. and Worsnop, D. R.: Real-Time Methods for Estimating Organic Component Mass Concentrations from Aerosol Mass Spectrometer Data, Environ. Sci. Technol., 45(3), 910–916, doi:10.1021/es102951k, 2011.

Pankow, J. F.: An absorption model of gas/particle partitioning of organic compounds in the atmosphere, Atmos. Environ., 28(2), 185–188, doi:10.1016/1352-2310(94)90093-0, 1994.

Park, K., Cao, F., Kittelson, D. B. and McMurry, P. H.: Relationship between Particle Mass and Mobility for Diesel Exhaust Particles, Environ. Sci. Technol., 37(3), 577–583, doi:10.1021/es025960v, 2003.

Pope, C. A. and Dockery, D. W.: Health effects of fine particulate air pollution: lines that connect, J. Air Waste Manag. Assoc. 1995, 56(6), 709–742, 2006.

Presto, A. A., Hennigan, C. J., Nguyen, N. T. and Robinson, A. L.: Determination of Volatility Distributions of Primary Organic Aerosol Emissions from Internal Combustion Engines Using Thermal Desorption Gas Chromatography Mass Spectrometry, Aerosol Sci. Technol., 46(10), 1129–1139, doi:10.1080/02786826.2012.700430, 2012.

Ranjan, M., Presto, A. A., May, A. A. and Robinson, A. L.: Temperature Dependence of Gas–Particle Partitioning of Primary Organic Aerosol Emissions from a Small Diesel Engine, Aerosol Sci. Technol., 46(1), 13–21, doi:10.1080/02786826.2011.602761, 2012.

Robert, M. A., VanBergen, S., Kleeman, M. J. and Jakober, C. A.: Size and composition distributions of particulate matter emissions: part 1--light-duty gasoline vehicles, J. Air Waste Manag. Assoc. 1995, 57(12), 1414–1428, 2007.

Robinson, A. L., Donahue, N. M., Shrivastava, M. K., Weitkamp, E. A., Sage, A. M., Grieshop, A. P., Lane, T. E., Pierce, J. R. and Pandis, S. N.: Rethinking Organic Aerosols: Semivolatile Emissions and Photochemical Aging, Science, 315(5816), 1259–1262, doi:10.1126/science.1133061, 2007.

Robinson, A. L., Grieshop, A. P., Donahue, N. M. and Hunt, S. W.: Updating the Conceptual Model for Fine Particle Mass Emissions from Combustion Systems Allen L. Robinson, J. Air Waste Manag. Assoc., 60(10), 1204–1222, doi:10.3155/1047-3289.60.10.1204, 2010.

Roth, C. M., Goss, K.-U. and Schwarzenbach, R. P.: Sorption of a diverse set of organic vapors to urban aerosols, Environ. Sci. Technol., 39(17), 6638–6643, 2005.

Saha, P. K. and Grieshop, A. P.: Exploring Divergent Volatility Properties from Yield and Thermodenuder Measurements of Secondary Organic Aerosol from α-Pinene Ozonolysis, Environ. Sci. Technol., 50(11), 5740–5749, doi:10.1021/acs.est.6b00303, 2016.

Saha, P. K., Khlystov, A. and Grieshop, A. P.: Determining Aerosol Volatility Parameters Using a “Dual Thermodenuder” System: Application to Laboratory-Generated Organic Aerosols, Aerosol Sci. Technol., 49(8), 620–632, doi:10.1080/02786826.2015.1056769, 2015.

Saha, P. K., Khlystov, A., Snyder, M. G. and Grieshop, A. P.: Characterization of air pollutant concentrations, fleet emission factors, and dispersion near a North Carolina interstate freeway across two seasons, Atmos. Environ., under review, 2017a.

Saha, P. K., Khlystov, A., Yahya, K., Zhang, Y., Xu, L., Ng, N. L. and Grieshop, A. P.: Quantifying the volatility of organic aerosol in the southeastern US, Atmos Chem Phys, 17(1), 501–520, doi:10.5194/acp-17-501-2017, 2017b.

Saleh, R., Khlystov, A. and Shihadeh, A.: Determination of Evaporation Coefficients of Ambient and Laboratory-Generated Semivolatile Organic Aerosols from Phase Equilibration Kinetics in a Thermodenuder, Aerosol Sci. Technol., 46(1), 22–30, doi:10.1080/02786826.2011.602762, 2012.

Saleh, R., Donahue, N. M. and Robinson, A. L.: Time Scales for Gas-Particle Partitioning Equilibration of Secondary Organic Aerosol Formed from Alpha-Pinene Ozonolysis, Environ. Sci. Technol., 47(11), 5588–5594, doi:10.1021/es400078d, 2013.

Schwarz, J. P., Gao, R. S., Fahey, D. W., Thomson, D. S., Watts, L. A., Wilson, J. C., Reeves, J. M., Darbeheshti, M., Baumgardner, D. G., Kok, G. L., Chung, S. H., Schulz, M., Hendricks, J., Lauer, A., Kärcher, B., Slowik, J. G., Rosenlof, K. H., Thompson, T. L., Langford, A. O., Loewenstein, M. and Aikin, K. C.: Single-particle measurements of midlatitude black carbon and light-scattering aerosols from the boundary layer to the lower stratosphere, J. Geophys. Res. Atmospheres, 111(D16), D16207, doi:10.1029/2006JD007076, 2006.

Shiraiwa, M., Kondo, Y., Moteki, N., Takegawa, N., Miyazaki, Y. and Blake, D. R.: Evolution of mixing state of black carbon in polluted air from Tokyo, Geophys. Res. Lett., 34(16), L16803, doi:10.1029/2007GL029819, 2007.

Shrivastava, M. K., Lipsky, E. M., Stanier, C. O. and Robinson, A. L.: Modeling Semivolatile Organic Aerosol Mass Emissions from Combustion Systems, Environ. Sci. Technol., 40(8), 2671–2677, doi:10.1021/es0522231, 2006.

Stephens, M., Turner, N. and Sandberg, J.: Particle identification by laser-induced incandescence in a solid-state laser cavity, Appl. Opt., 42(19), 3726–3736, doi:10.1364/AO.42.003726, 2003.

Subramanian, R., Kok, G. L., Baumgardner, D., Clarke, A., Shinozuka, Y., Campos, T. L., Heizer, C. G., Stephens, B. B., de Foy, B., Voss, P. B. and Zaveri, R. A.: Black carbon over Mexico: the effect of atmospheric transport on mixing state, mass absorption cross-section, and BC/CO ratios, Atmos Chem Phys, 10(1), 219–237, doi:10.5194/acp-10-219-2010, 2010.

Tiitta, P., Miettinen, P., Vaattovaara, P., Joutsensaari, J., Petäjä, T., Virtanen, A., Raatikainen, T., Aalto, P., Portin, H., Romakkaniemi, S., Kokkola, H., Lehtinen, K. E. J., Kulmala, M. and Laaksonen, A.: Roadside aerosol study using hygroscopic, organic and volatility TDMAs: Characterization and mixing state, Atmos. Environ., 44(7), 976–986, doi:10.1016/j.atmosenv.2009.06.021, 2010.

Wang, J. M., Jeong, C.-H., Zimmerman, N., Healy, R. M., Hilker, N. and Evans, G. J.: Real-World Emission of Particles from Vehicles: Volatility and the Effects of Ambient Temperature, Environ. Sci. Technol., doi:10.1021/acs.est.6b05328, 2017.

Willis, M. D., Healy, R. M., Riemer, N., West, M., Wang, J. M., Jeong, C.-H., Wenger, J. C., Evans, G. J., Abbatt, J. P. D. and Lee, A. K. Y.: Quantification of black carbon mixing state from traffic: implications for aerosol optical properties, Atmos Chem Phys, 16(7), 4693–4706, doi:10.5194/acp-16-4693-2016, 2016.

Zhang, K. M., Wexler, A. S., Zhu, Y. F., Hinds, W. C. and Sioutas, C.: Evolution of particle number distribution near roadways. Part II: the “Road-to-Ambient” process, Atmos. Environ., 38(38), 6655–6665, doi:10.1016/j.atmosenv.2004.06.044, 2004.

Zhang, R., Wang, G., Guo, S., Zamora, M. L., Ying, Q., Lin, Y., Wang, W., Hu, M. and Wang, Y.: Formation of Urban Fine Particulate Matter, Chem. Rev., 115(10), 3803–3855, doi:10.1021/acs.chemrev.5b00067, 2015.

Zhu, Y., Hinds, W. C., Kim, S. and Sioutas, C.: Concentration and Size Distribution of Ultrafine Particles Near a Major Highway, J. Air Waste Manag. Assoc., 52(9), 1032–1042, doi:10.1080/10473289.2002.10470842, 2002.

Table 1: TD-derived particle volatility distributions (at 298 K) at 10 m and 220 m downwind distance from the highway I-40 during summer and winter. Laboratory-derived gasoline POA distribution by May et al. (2013a) is also listed.

logC* at 298K	[a]TD-derived f_i distribution				[b]Gasoline POA (May et al. 2013)
	10 m (Summer)	220 m (Summer)	10 m (Winter)	220 m (Winter)	
-4	0.07	0.10	0.18	0.28	
-3	0.13	0.21	0.07	0.08	
-2	0.16	0.20	0.14	0.20	0.14
-1	0.27	0.37	0.15	0.30	0.13
0	0.12	0.06	0.27	0.09	0.15
1	0.25	0.06	0.20	0.06	0.26
2					0.15
3					0.03
4					0.03
5					0.01
6					0.11

[a]TD-fitted particle-phase distributions (x_i) with γ_{e} = 0.25 and ΔH_{vap} = 100 KJ mol^{-1} (reported in Table S2) are converted to total (gas+particle) distribution (f_i) under gas-particle equilibrium condition and assuming a total aerosol loading of ~ 5 µg m^{-3}. (Conversion equations are given in S1, Sec. S3).

[b]Chromatographic analysis

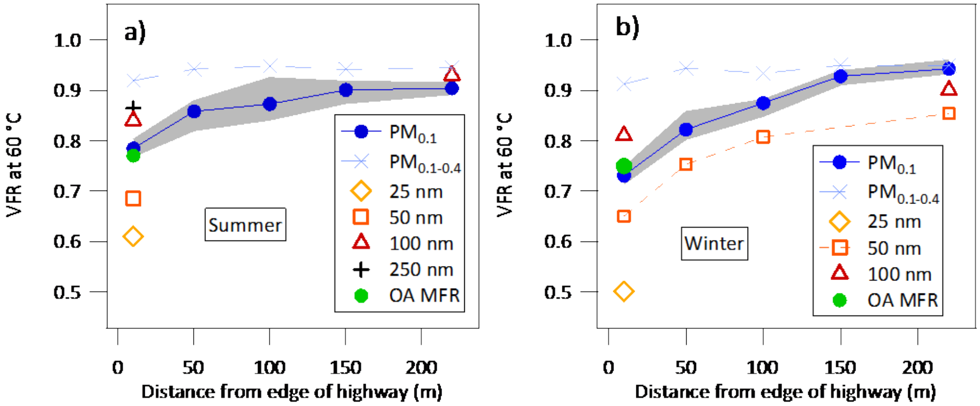

Figure 1: Campaign-average downwind evolution of volume fraction remaining (VFR) of near-road particles after heating at 60 °C in a TD (Rt = 30 s) during (a) summer, and (b) winter. VFR of size-selected particles (e.g., 25, 50, 100, 250 nm) obtained from V-TDMA measurements. VFR of $PM_{0.1}$ and $PM_{0.1-0.4}$ estimated from integrated SMPS volume between 10-100 nm and 100-400 nm, respectively. OA MFR was measured using a TD/ACSM system (Rt = 30 s) in the near-road trailer. The shaded area represents interquartile range of all measurements for each season.

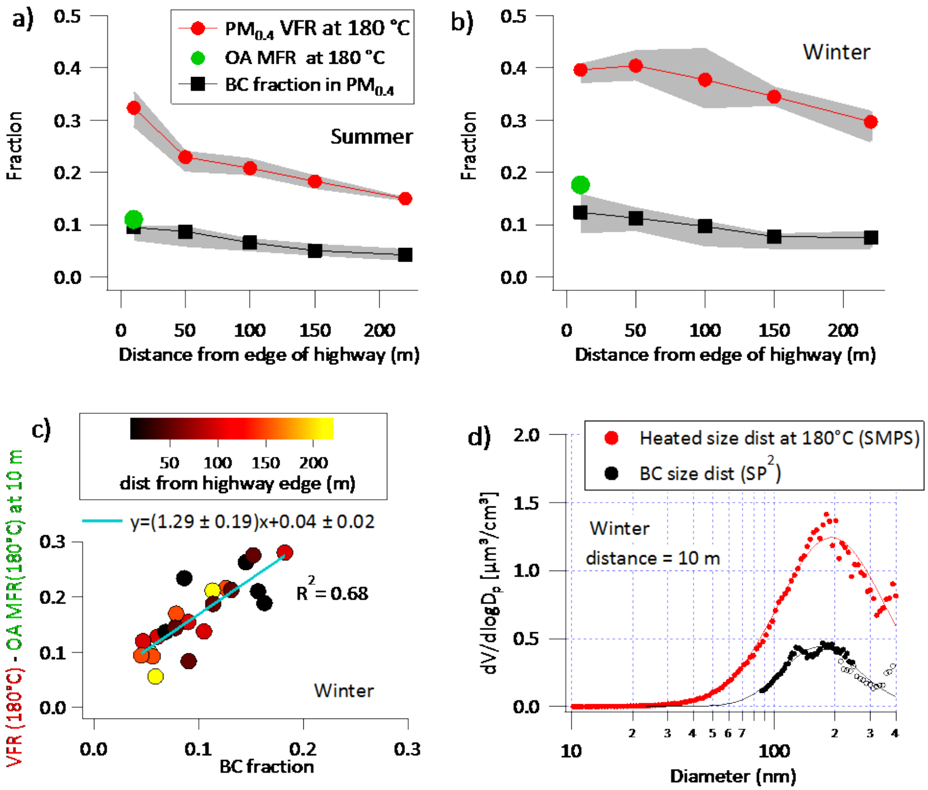

Figure 2: Campaign-average downwind evolution of volume fraction remaining (VFR) of $PM_{0.4}$ (integrated SMPS volume over 10-400 nm) at 180 °C in a TD (Rt = 30 s) and black carbon (BC) fraction in $PM_{0.4}$ during (a) summer, and (b) winter. Points are mean and the shaded area represents interquartile range. OA MFR was measured using a TD/ACSM system (Rt = 30 s) only in the near-road trailer. (c) Correlation between the BC fraction and VFR of $PM_{0.4}$ (at 180 ºC) at various downwind distances after subtracting OA MFR (at 180ºC) measured at 10 m. (d) Comparison of SMPS-measured thermodenuded size distribution at 180 ºC and SP2-measured BC size distribution.

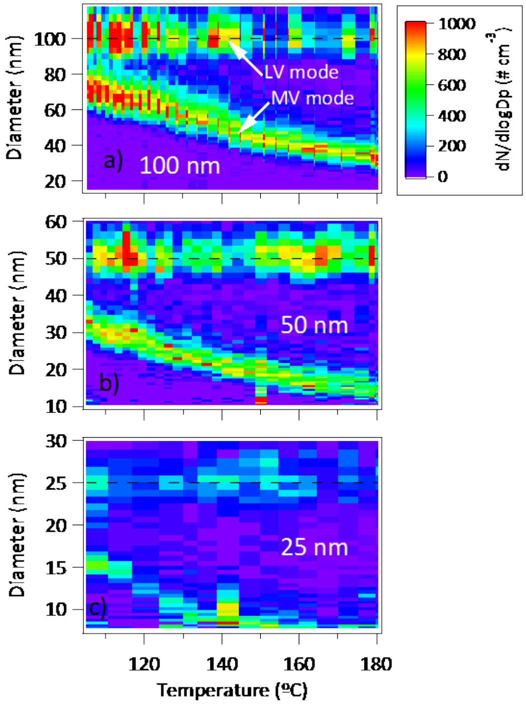

Figure 3: Average V-TDMA volatility spectra of 25, 50, and 100 nm particles collected 10 m from I-40 during summer. Figure S9 shows similar plots for the winter data set.

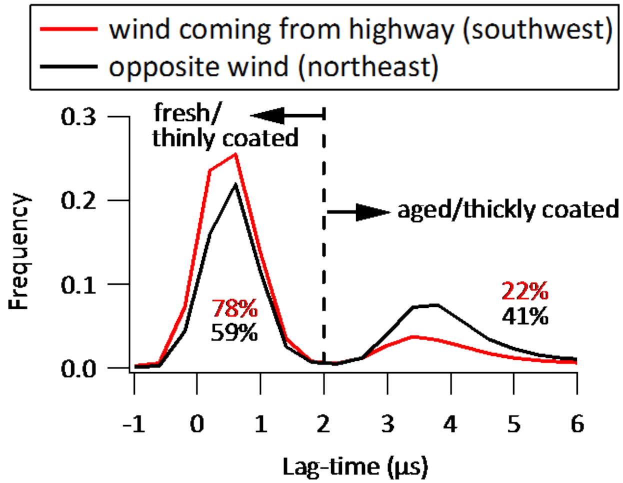

Figure 4: Campaign-average frequency distributions (histograms) of SP2 lag-time ($\Delta\tau$) for refractory BC-containing particles measured during periods with winds from the highway (red) or from the opposite direction (black). Measurements were collected at 10 m distance from the highway in winter.

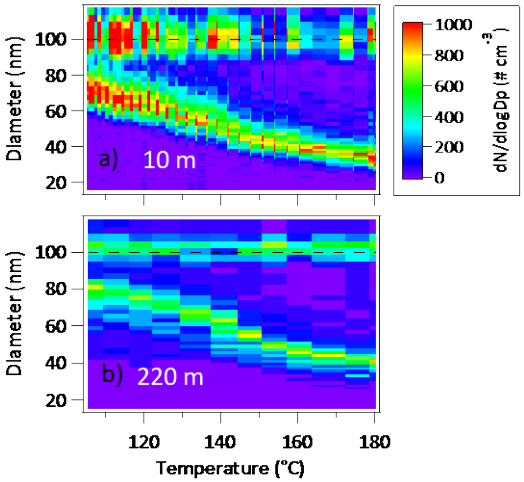

Figure 5: Similar to Figure 3 showing average volatility spectra of 100 nm particles at 10 m and 220 m downwind of the highway. Measurements were collected during transect runs in summer.

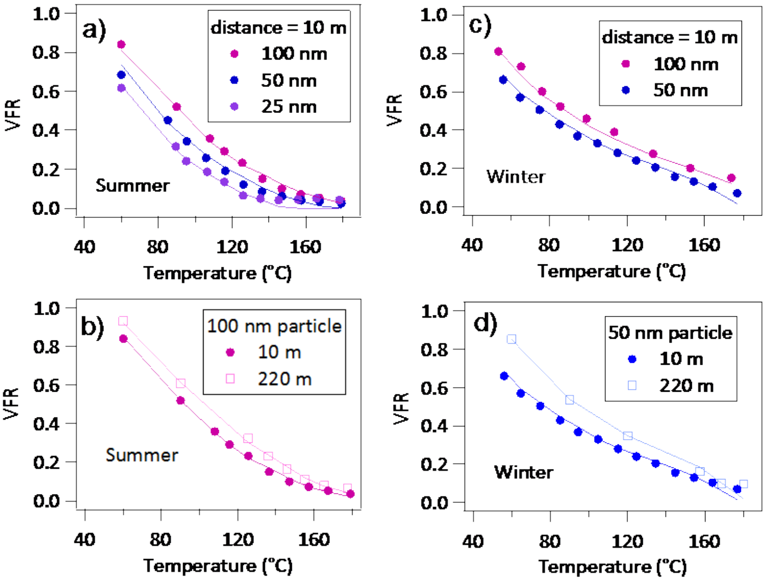

Figure 6: Campaign-average measured (points) and modeled (line) thermograms for different sized particles measured at 10 m and 220 m downwind during summer (a-b) and winter (c-d). Model lines are shown using the best fitted volatility distributions listed in Tables 1 and S2, and ΔH_{vap} = 100 KJ mol^{-1} and γ_{e} = 0.25.

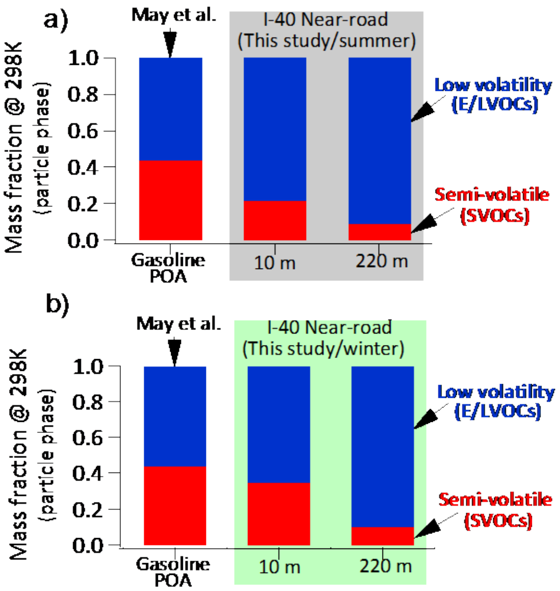

Figure 7: Comparison of volatility classification of near-road particles measured at 10 m and 220 m (this study) for a) summer, and b) winter at a reference temperature of 25ºC. Distributions of particle-phase material are shown using two broad volatility categories. Also shown in both panels is the POA distribution from gasoline vehicle exhaust by May et al. (2013a) under typical near-road aerosol loading (C_{OA}~5 µg m^{-3}).

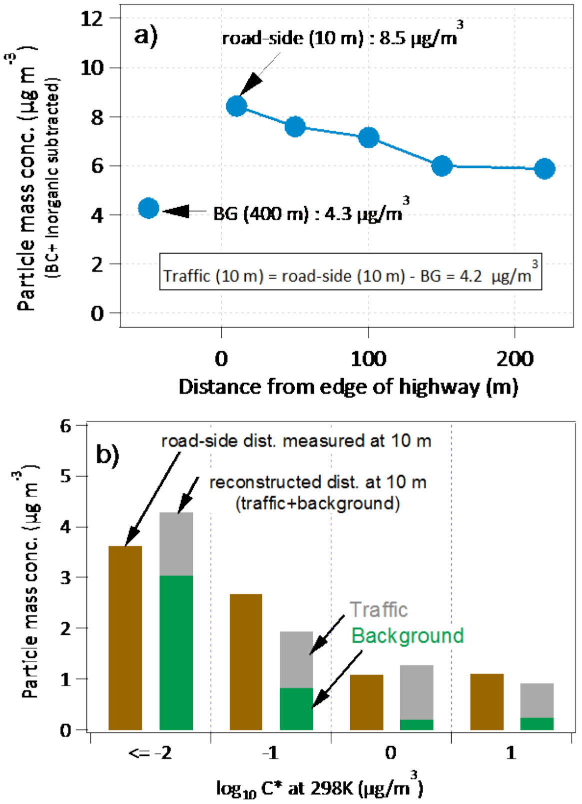

Figure 8: Comparison of measured road-side volatility distribution (at 10 m) with a reconstructed distribution using traffic and background contribution. Analysis conducted using an example data set from a transect measurement on June 12, 2015 (summer), with the wind consistently coming off of the highway. (a) Measured upwind (background) and downwind concentrations of particle mass loading as a function of distances from the highway. (b) Comparison of measured road-side volatility distribution (at 10 m) with the reconstructed distribution using laboratory-measured POA volatility distribution from May et al. (2013) as representative of traffic particles and our measured volatility distribution at our far-road location (220 m) as a representative of background particles.

Supplementary Information (SI) of

Downwind evolution of the volatility and mixing state of near-road aerosols near a US interstate highway

Provat Kumar Saha[1], Andrey Khlystov[2], and Andrew Patrick Grieshop[1]

[1]Department of Civil, Construction and Environmental Engineering, North Carolina State University, Raleigh, North Carolina, USA

[2]Division of Atmospheric Sciences, Desert Research Institute, Reno, Nevada, USA

Correspondence to: A. P. Grieshop (apgriesh@ncsu.edu)

S1: Supplementary figures

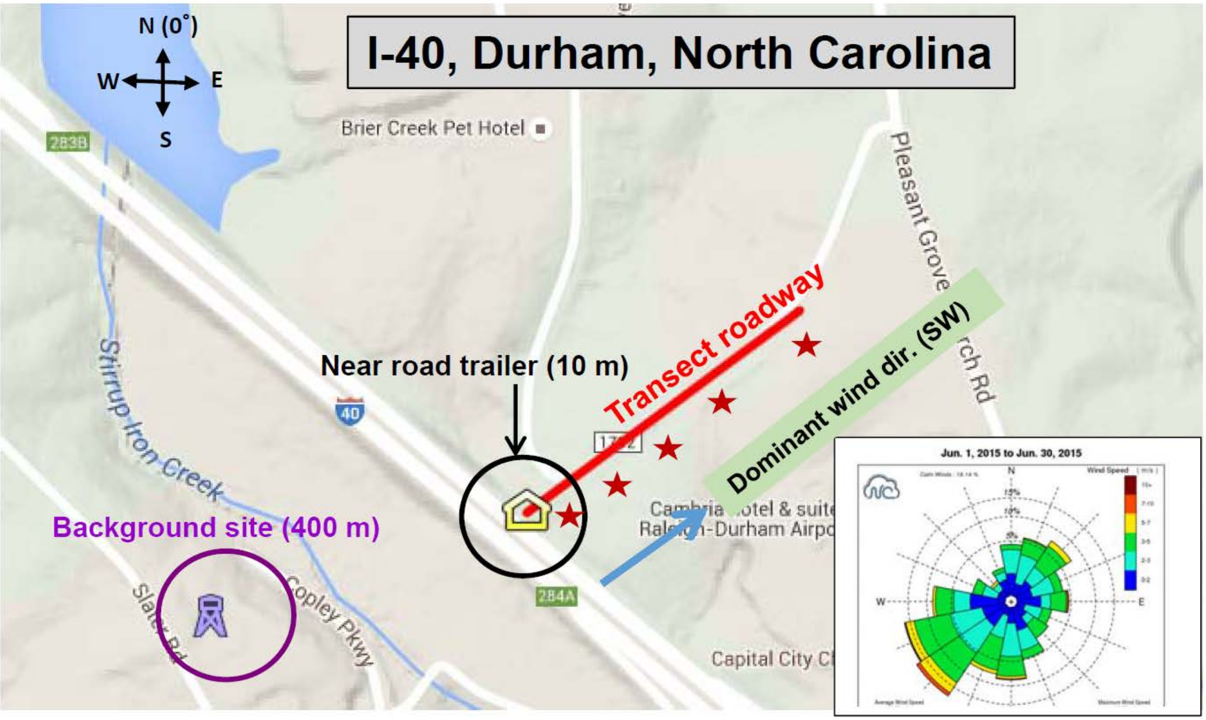

Figure S1: Study area map showing near-road trailer, transect roadway and upwind background site. Wind rose plot (inset) is shown for the I-40 summer campaign period (June 1 to June 30, 2015). Image: Google Maps

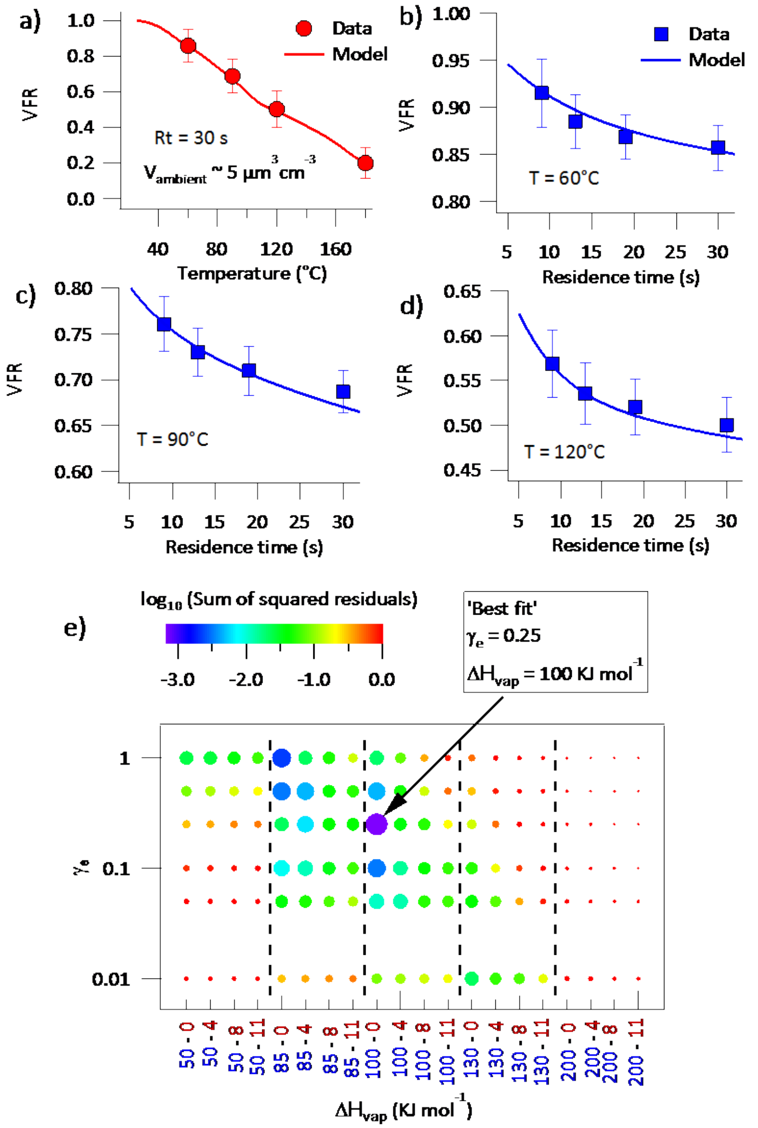

Figure S2: (a-d) Measured (point) and modeled (line) campaign-average VFR of PM$_{0.4}$ (integrated volume; 10-400 nm) as a function of TD temperatures and residence times. Measurements were collected in summer 2015 at 10 m distance from the highway. The point is mean, and error bar is ± one standard deviation (~15 minute time resolution data) at each temperature and Rt condition. (e) The goodness of fit (sum of squared residuals; SSR) associated with evaporation kinetics model fits to campaign average observations over a wide ranging (ΔH_{vap} γ_e) space. A larger marker size indicates a better fit. The x-axis of panel (e) represents ΔH_{vap} as, ΔH_{vap} = intercept-slope (log$_{10}C^*$) (e.g., 50-0 on x-axis indicates intercept = 50 and slope = 0). Fitting approach is described in detail in Saha et al. (2015). Model lines in panels (a-d) are shown using the 'best fit' parameter values (ΔH_{vap} = 100 kj mol^{-1}, γ_e = 0.25, and corresponding fitted volatility distribution).

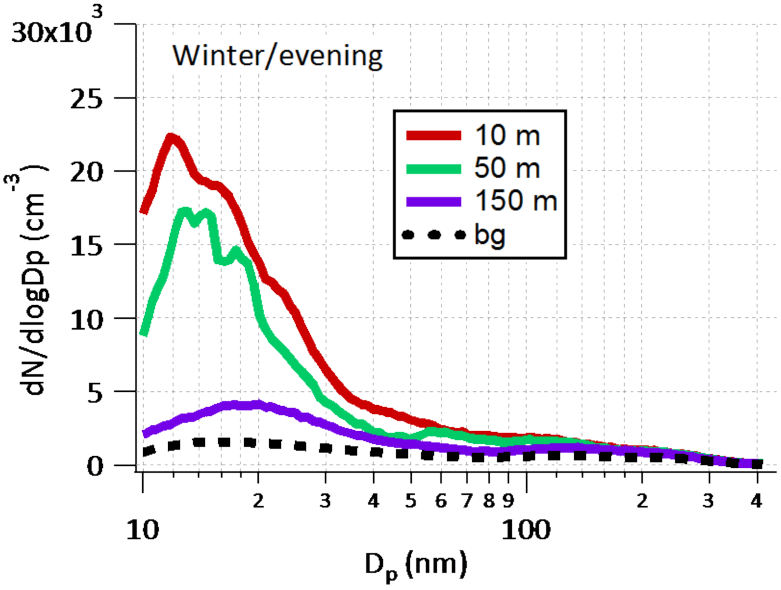

Figure S3: Particle number size distributions at different distances from highway. Example data are shown from a transect measurement during I-40 the winter campaign. The background (bg) measurement was collected at approximately 400 m ‘upwind’ from the main roadside monitor station on the opposite side of I-40.

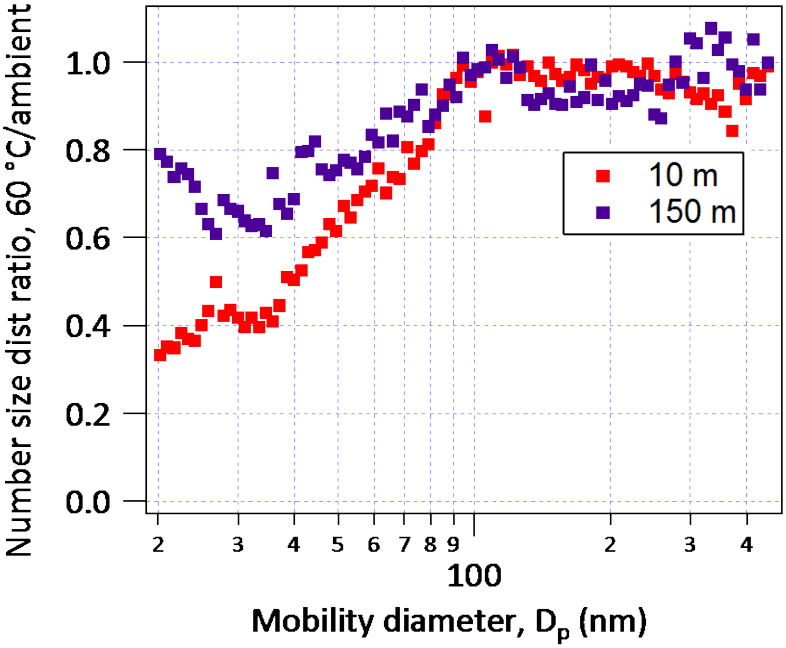

Figure S4: Ratio of particle number size distributions (dN/dlogDp) after heating at 60ºC in a thermodenuder (TD) to that at ambient temperature. Example measurements are shown from a typical transect run. Before ratio estimation, particle loss correction factors (as a function of size) were applied to the TD data.

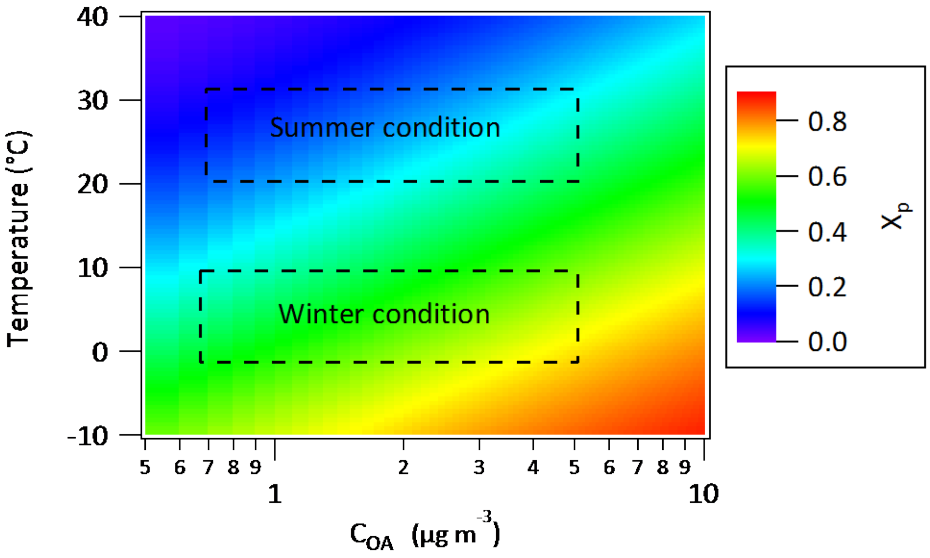

Figure S5: Temperature sensitivity of gas-particle partitioning of semi-volatile emissions from motor vehicles. Partitioning calculation uses gasoline POA volatility distribution from May et al. (2013) (TD-GC-MS derived median distribution) and △Hvap from Ranjan et al. (2012) and method as described in May et al.(2013) and Donahue et al. (2006). X_p refer the fraction of semi-volatile organic mass in the particle-phase.

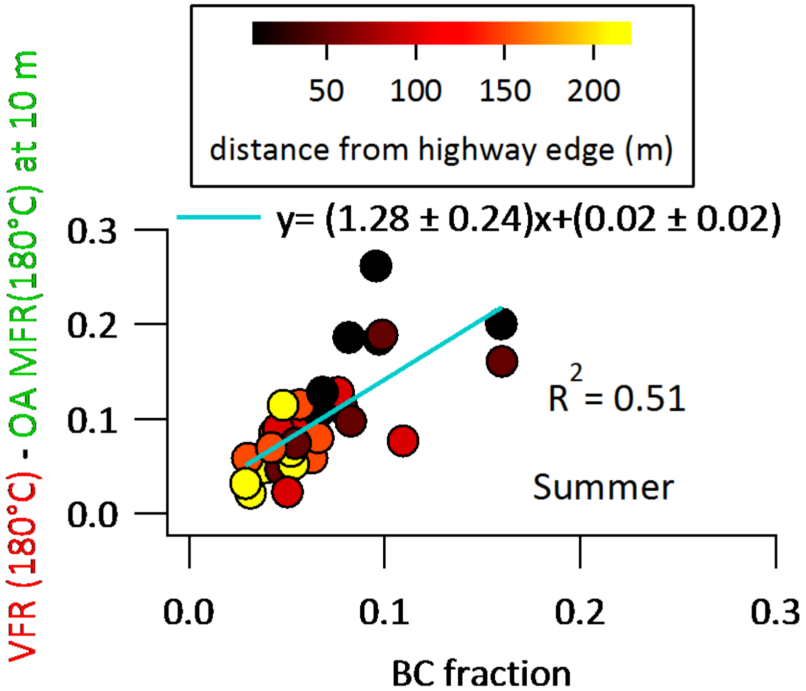

Figure S6: Similar to Figure 2(c) in main text, showing analysis for the summer data set. Correlation between the downwind evolution of BC fraction and VFR of $PM_{0.4}$ (at 180 ºC) after subtracting OA MFR (at 180ºC) measured at 10 m using TD/ACSM.

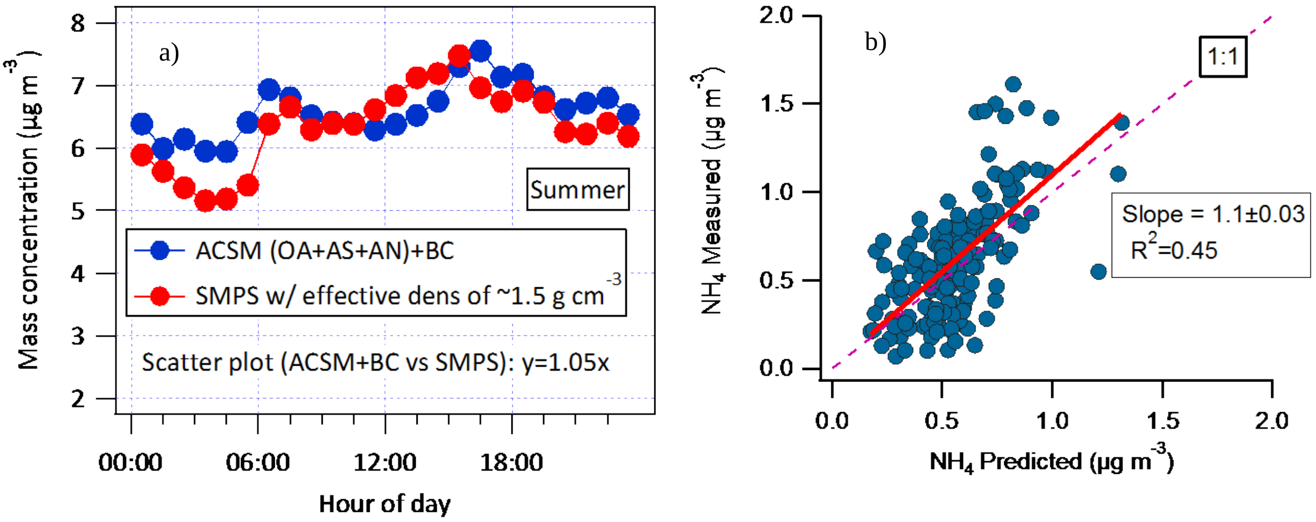

Figure S7: a) Comparison of diurnal average submicron ambient aerosol mass concentrations measured by SMPS with the concentrations measured by ACSM [organic aerosol (OA) + ammonium sulfate (AS) + ammonium nitrate (AN)] + PAX [black carbon (BC)]. Campaign-average diurnal profile is shown from summer campaign. ACSM data were analyzed using a collection efficiency (CE) of 1 for all species. AS mass concentration (m_{as}) is calculated as $\frac{\mathbf{132}}{\mathbf{96}} \times m_{SO4}$, where m_{SO4} is the mass concentration of sulfate (SO_4). AN mass concentration (m_{an}) is calculated as $\frac{\mathbf{80}}{\mathbf{62}} \times m_{NO3}$, where m_{NO3} is the mass concentration of nitrate (SO_4). This calculation assumes that aerosols are neutral. An ammonium balance can provide insights into the validity of assumption of neutral aerosol. Panel (b) shows NH4 measured vs. NH_4 predicted plot. The NH4 predicted is estimated as: NH4 predicted = 2*(18/98)*SO4 + (18/63)*NO3 + (18/35)*Cl, where the fractional amounts correspond to the molecular weights of the relevant species. An acidity plot (of measured vs. predicted NH4) has an average slope closer to ~1 (1.1±0.03), indicating an ammonium balance. Therefore, assumption of neutral aerosols at the measurement location was reasonable. SMPS mass concentrations in panel (a) were based on an estimated effective density of submicron aerosols of 1.5 cm$^{-3.}$ The effective density is calculated by weighting fractional contribution of different species (e.g., campaign average: OA ~74%, AS ~13%, AN ~7%, and BC ~6%) with their respective densities. Assumed densities for AS, AN, and BC were 1.77, 1.72 and 1.8 g cm^{-3}, respectively. An effective density of OA of 1.45 g cm^{-3}, estimated from a parameterization by Kuwata et al. (2012) using elemental composition (O:C; H:C). Kuwata et al. (2012) parameterization for OA density was developed based on laboratory data with negligible BC or NO3. It should be noted that Kuwata et al. applied their parameterization to data from the AMAZE campaign, which had an average OA fraction of 0.8 (versus 0.74 for our data), and found that the results agreed well with their measured density. Since our mass comparison based on application of this density to SMPS-measured volume and ACSM+BC mass showed good agreement (Fig. S7a), this indicates our overall estimated effective density, on which OA density has the largest influence, is well constrained.

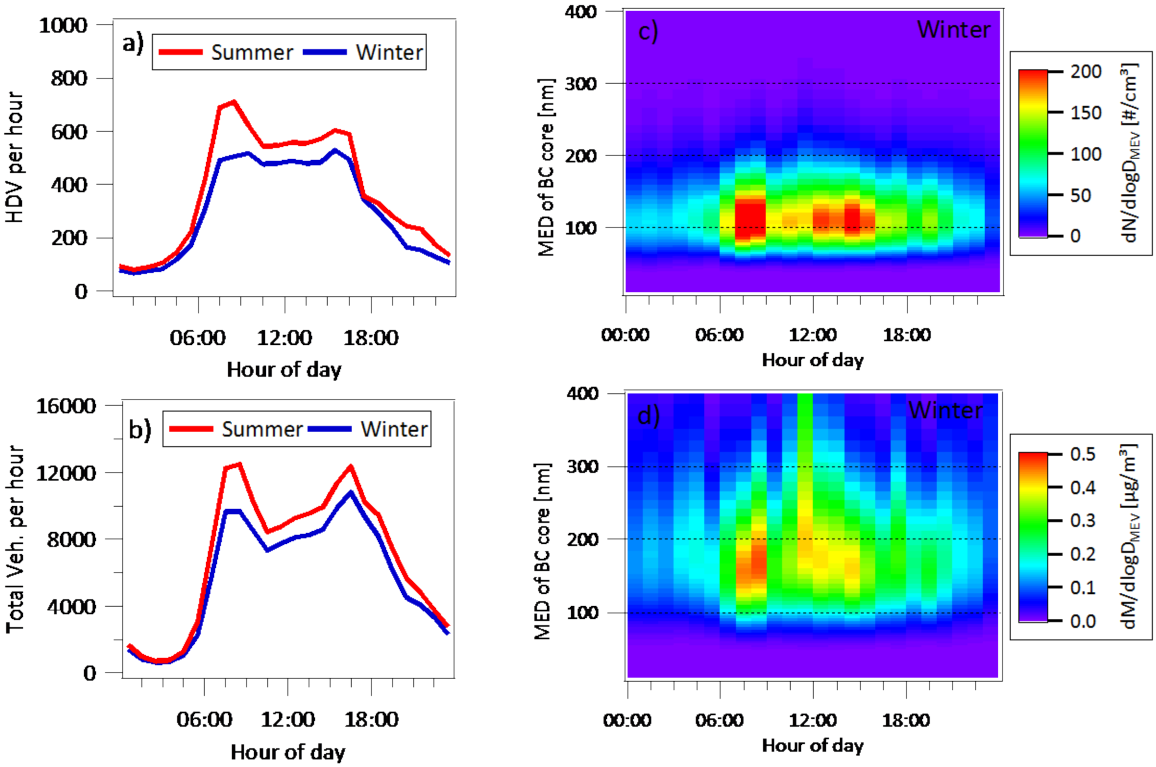

Figure S8: (a-b) Campaign-average diurnal profile of traffic volume: a) heavy duty vehicle (HDV), b) total vehicle. (c-d) Campaign-average diurnal profile of SP2-measured BC size distribution: c) number-weighted distribution, d) mass-weighted distribution; MED is the mass equivalent diameter. SP2 data were collected at the roadside trailer (10 m from highway edge) during the I-40 winter campaign only.

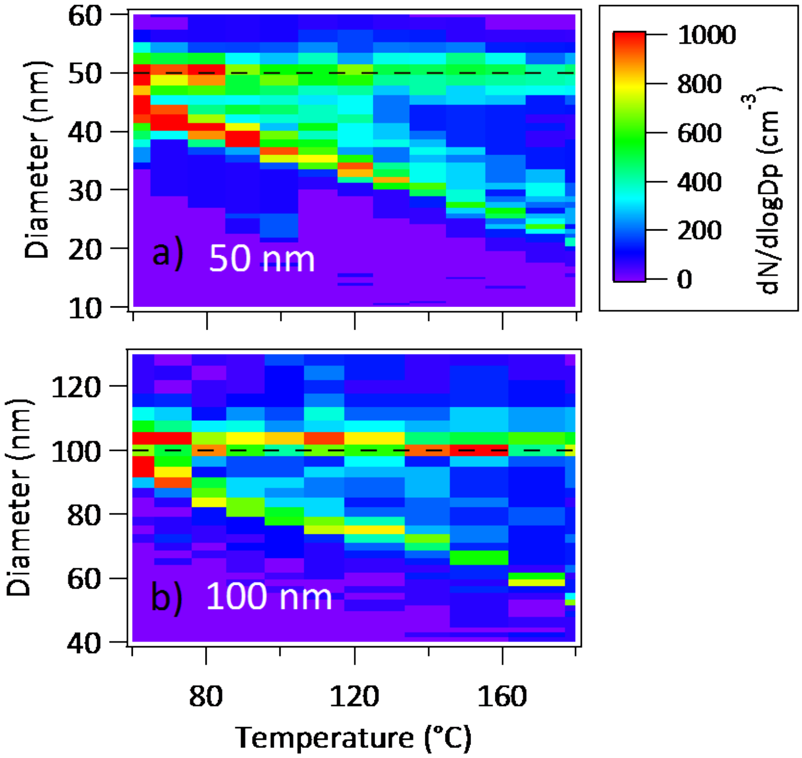

Figure S9: Similar to Figure 3 in main text, showing average volatility spectra of 50, and 100 nm particles collected at 10 m distance during the I-40 winter campaign.

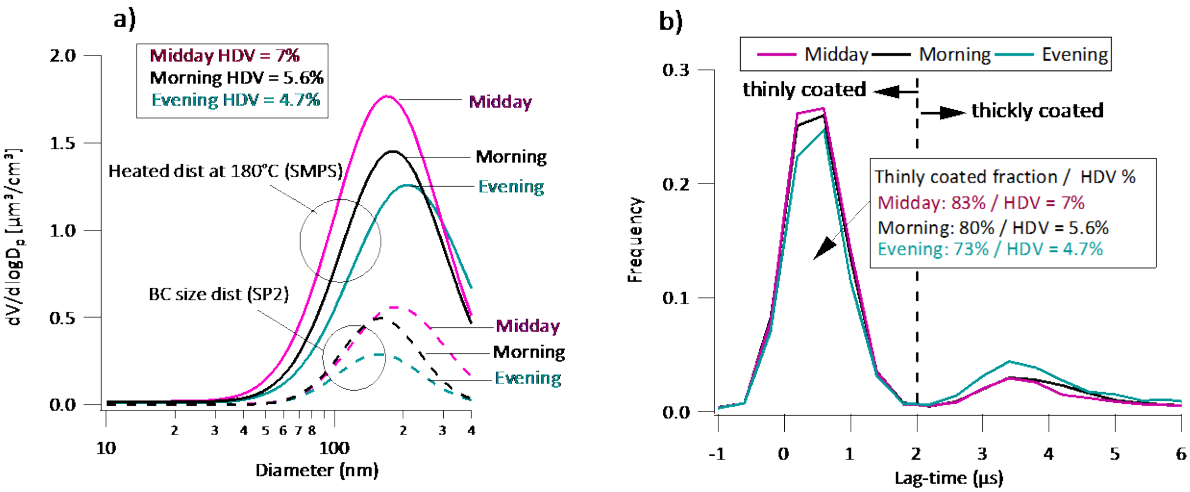

Figure S10: (a) Temporal variation of SP2-measured BC size distribution and volume-weighted SMPS size distribution after heating at 180 ºC in a thermodenuder. (b) Temporal variation of the frequency distributions (histograms) of SP2 lag-time (Δτ). The analysis shown here is based on an example data set collected at 10 m downwind distance on February 10, 2016 with the wind consistently coming off of the highway.

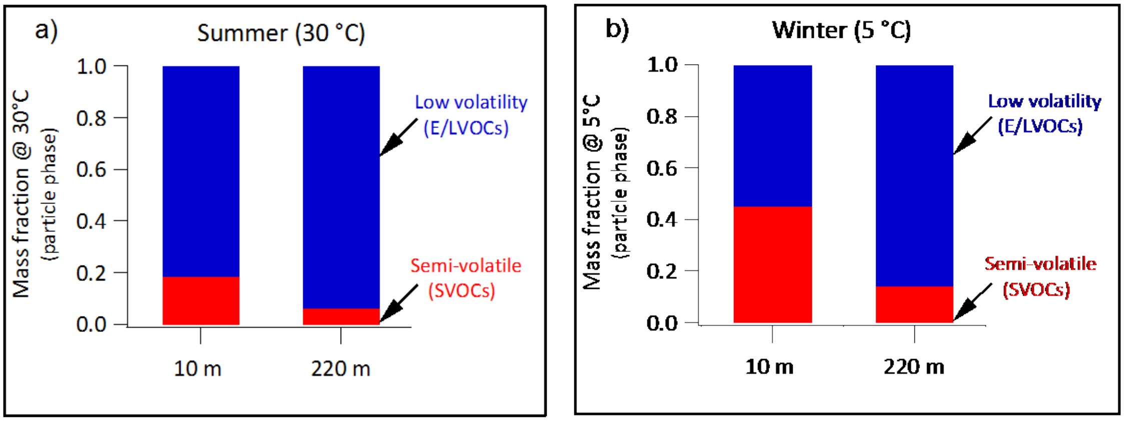

Figure S11: Similar to Figure 7 in the main text, showing volatility classification of near-road particles measured at 10 m and 220 m at campaign-average ambient temperature of ~5 ºC in winter and ~30ºC in summer. Distributions of particle-phase material are shown using two broad volatility categories. Partitioning calculation used a ΔH_{vap} of 100 kj mol^{-1}, Clausius–Clapeyron equation and equlibrium partitioning theory (Donahue et al., 2006) for estimating volatility distributions at campaign-average ambient temperatures.

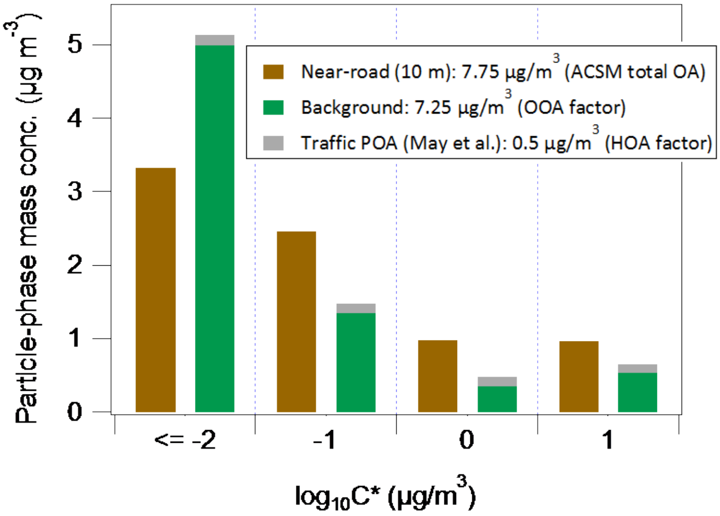

Figure S12: Similar to Figure 8b in the main text. In this analysis, traffic and background OA are taken from tracer m/z based factor analysis (Ng et al., 2011) of ACSM-measured mass spectra data at the roadside location. Hydrocarbon-like OA (HOA) is considered as traffic OA and oxygenated-OA (OOA) is considered as background OA. To be consistent with Figure 8, this analysis also considered data from the morning period on June 12, 2015. Figure shows comparison of measured road-side volatility distribution (at 10 m) with the reconstructed distribution using laboratory-measured POA volatility distribution by May et al. (2013) as representative of traffic particles and our measured volatility distribution at far-road location (220 m) as a representative of background particles

S2: Supplementary tables

Table S1: Assumed TD kinetic model input parameters*

Parameters	Value
Diffusion coefficient (m^2 s^{-1})	5 E-06
Surface tension (J m^{-2})	0.05
Molecular weight (MW) g mol^{-1}	200

*assumed values similar as used in May et al. (2013) for TD modelling

Table S2: TD-derived volatility distribution (at 25ºC) of near-road aerosols (particle-phase distribution) at 10 m and 220 m downwind distance from the highway I-40 during summer and winter

logC* at 298K	[a]Particle-phase distribution (x_i)			
	Derived from fitting of observed evaporation of size-selected particles			
	10 m (summer)	220 m (summer)	10 m (winter)	220 m (winter)
	Combined (25,50,100 nm)	100 nm	Combined (50,100 nm)	50 nm
-4	0.09	0.11	0.22	0.30
-3	0.16	0.22	0.08	0.08
-2	0.2	0.21	0.17	0.21
-1	0.33	0.38	0.18	0.31
0	0.12	0.05	0.27	0.08
1	0.1	0.02	0.08	0.02

[a]Reported volatility distributions are fitted with γ_{e} = 0.25 and ΔH_{vap} = 100 KJ mol^{-1} combination

S3: Conversion equations for TD-fitted particle-phase distribution (x_i) to total (gas+particle) distribution (f_i) under a gas-particle equilibrium condition.

$$C_{tot,\mathrm{i}} = \frac{x_i C_{OA}}{\left(1+\frac{C_i^*}{C_{OA}}\right)^{-1}} \qquad \text{[Eq. S1]}$$

$$f_i = \frac{C_{tot,\mathrm{i}}}{\sum C_{tot,\mathrm{i}}} \qquad \text{[Eq. S2]}$$

Here,

$C_{tot,i}$ (µg m^{-3}): total vapor- and particle-phase mass concentration of compound *i*,

C^*_i (µg m^{-3}): effective saturation concentration of compound *i* at a reference temperature (T_{ref})

C_{OA} (µg m^{-3}): total particle-phase organic mass concentration

x_i : mass fraction of compound i found in the particle phase

f_i : fraction of the total vapor and particle-phase contributed by species *i*

Temperature dependent C_i^* is estimated from the Clausius-Clapyeron Equation (Eq. S3)

$$C_i^*(T) = C_i^*(T_{ref})\exp\left[\frac{\Delta H_{vap,i}}{R}\left(\frac{1}{T_{ref}}-\frac{1}{T}\right)\right]\frac{T_{ref}}{T} \qquad \text{[Eq. S3]}$$

where ΔH_{vap} (kJ mol^{-1}) is the enthalpy of vaporization, *R* the gas constant, and T_{ref} the reference temperature (298 K).

S4: Reconstruction of road-side OA volatility distribution combining traffic and background volatility distribution.

This section describes the analysis approach step-by step those are used for reconstruction of road-side OA volatility distribution combining traffic and background volatility distribution, as shown in Figure 8 and discussed in Sec. 3.4 (main paper)

a) Approximate OA mass concentrations at different distance from the highway are estimated from SMPS measurements as:
SMPS total mass conc. (function of distance) – BC (function of distance) – inorganics (ACSM at fixed location).
For example, Roadside OA mass at 10 m = SMPS total mass (10 m) - BC (10 m) - inorganics (ACSM at fixed site);
Background OA = SMPS total mass (background) - BC (background) - inorganics (ACSM at fixed site).
An effective density of 1.5 g cm^{-3} (Fig. S7) was used to convert SMPS total volume to total mass.

b) Traffic OA at a downwind road-side location is estimated as: total road-side OA - upwind background OA
For example, traffic OA (at 10 m downwind) = total road-side OA (at 10 m downwind) – upwind background OA

c) Distribution of road-side OA, traffic OA, and background OA in different volatility bins (i) are calculated as:
M_{OA} (road-side at 10 m)$_i$ = road-side OA mass at 10 m × (TD volatility distribution at 10 m)$_i$
M_{OA} (background)$_i$ = background OA mass × (TD volatility distribution at 220 m)$_i$
M_{OA} (traffic at 10 m)$_i$ = traffic OA mass at 10 m × (Traffic POA volatility distribution from May et. al.)$_i$

d) Reconstructed roadside OA volatility distribution is estimated as:
Reconstructed M_{OA} (road-side at 10 m)$_{i\,=}$ M_{OA} (traffic at 10 m)$_i$ + M_{OA} (background)$_i$
Finally, we compare this reconstructed distribution with our road-side distribution measured at 10 mm (see Figure 8b of main paper).

S5: Tracer m/z based factor analysis of ACSM data set

Tracer m/z based OA components are estimated following Ng et al. (2011) as: hydrocarbon-like OA (HOA ~ 13.4 × (C_{57} − 0.1 × C_{44})) and oxygenated OA (OOA ~ 6.6 × C_{44}), where C_{57} and C_{44} are the equivalent mass concentration of tracer ion m/z 57 and 44, respectively. Previous evaluation of this method has shown that it can reproduce the HOA and OOA concentrations to within ~30% of the results from detailed PMF analysis at most sites (Ng. et al. 2011). The estimated traffic-OA (HOA factor) contribution was found to be substantially lower (~5-10x) than that derived based on background-subtracted roadside concentrations measured by SMPS in combination with other data (e..g, Fig. 8a in the main text). Therefore, in analysis shown in Figure S12, the volatility of near-road particles is dominated by contribution from background particles and the combined distribution does a poor job of recreating the observed near-road volatility distribution.

Several factors likely contribute to this discrepancy. For one, since the correlation equations for tracer m/z based factor analysis are empirical (Ng et al., 2011), this method's accuracy and representativeness may be limited in many environments. Further, a substantial fraction of traffic-emitted smaller particles may fall outside of transmission window of ACSM (< 70 nm), but these small particles likely do not have significant contributions to overall mass contribution. On the other hand, measurements of fresh vehicle-emitted particles with an SMPS may be biased high to some extent due to the non-spherical morphology of fresh soot particles (DeCarlo et al., 2004; Maricq and Xu, 2004; Park et al., 2003). For example, effective densities of vehicle-emitted particles with mobility diameters of 200 nm may be <0.3 g cm^{-3}, a factor of 5 lower than that value assumed here (Maricq and Xu, 2004). The true estimates of traffic-OA likely fall between the ACSM-HOA and SMPS-based estimation. However, these two estimates may be considered as bounding cases. Further efforts should be made to investigate the closure of estimates from different instruments and approaches.

References

DeCarlo, P. F., Slowik, J. G., Worsnop, D. R., Davidovits, P. and Jimenez, J. L.: Particle Morphology and Density Characterization by Combined Mobility and Aerodynamic Diameter Measurements. Part 1: Theory, Aerosol Sci. Technol., 38(12), 1185–1205, doi:10.1080/027868290903907, 2004.

Donahue, N. M., Robinson, A. L., Stanier, C. O. and Pandis, S. N.: Coupled Partitioning, Dilution, and Chemical Aging of Semivolatile Organics, Environ. Sci. Technol., 40(8), 2635–2643, doi:10.1021/es052297c, 2006.

Kuwata, M., Zorn, S. R. and Martin, S. T.: Using Elemental Ratios to Predict the Density of Organic Material Composed of Carbon, Hydrogen, and Oxygen, Environ. Sci. Technol., 46(2), 787–794, doi:10.1021/es202525q, 2012.

Maricq, M. M. and Xu, N.: The effective density and fractal dimension of soot particles from premixed flames and motor vehicle exhaust, J. Aerosol Sci., 35(10), 1251–1274, doi:10.1016/j.jaerosci.2004.05.002, 2004.

May, A. A., Presto, A. A., Hennigan, C. J., Nguyen, N. T., Gordon, T. D. and Robinson, A. L.: Gas-particle partitioning of primary organic aerosol emissions: (1) Gasoline vehicle exhaust, Atmos. Environ., 77, 128–139, doi:10.1016/j.atmosenv.2013.04.060, 2013.

Ng, N. L., Canagaratna, M. R., Jimenez, J. L., Zhang, Q., Ulbrich, I. M. and Worsnop, D. R.: Real-Time Methods for Estimating Organic Component Mass Concentrations from Aerosol Mass Spectrometer Data, Environ. Sci. Technol., 45(3), 910–916, doi:10.1021/es102951k, 2011.

Park, K., Cao, F., Kittelson, D. B. and McMurry, P. H.: Relationship between Particle Mass and Mobility for Diesel Exhaust Particles, Environ. Sci. Technol., 37(3), 577–583, doi:10.1021/es025960v, 2003.

Ranjan, M., Presto, A. A., May, A. A. and Robinson, A. L.: Temperature Dependence of Gas–Particle Partitioning of Primary Organic Aerosol Emissions from a Small Diesel Engine, Aerosol Sci. Technol., 46(1), 13–21, doi:10.1080/02786826.2011.602761, 2012.

Saha, P. K., Khlystov, A. and Grieshop, A. P.: Determining Aerosol Volatility Parameters Using a “Dual Thermodenuder” System: Application to Laboratory-Generated Organic Aerosols, Aerosol Sci. Technol., 49(8), 620–632, doi:10.1080/02786826.2015.1056769, 2015.